Michigan Technological University

Create the Future Digital Commons @ Michigan Tech

Dissertations, Master's Theses and Master's Reports - Open

Dissertations, Master's Theses and Master's Reports

2014

SVPWM SWITCHING PATTERN FOR Z-SOURCE INVERTER, SIMULATION AND APPLICATION

Zhe Huang
Michigan Technological University

Follow this and additional works at: https://digitalcommons.mtu.edu/etds

Part of the Electrical and Computer Engineering Commons

Copyright 2014 Zhe Huang

Recommended Citation
Huang, Zhe, "SVPWM SWITCHING PATTERN FOR Z-SOURCE INVERTER, SIMULATION AND APPLICATION", Master's report, Michigan Technological University, 2014.
https://doi.org/10.37099/mtu.dc.etds/812

Follow this and additional works at: https://digitalcommons.mtu.edu/etds

Part of the Electrical and Computer Engineering Commons

SVPWM SWITCHING PATTERN FOR Z-SOURCE INVERTER, SIMULATION AND APPLICATION

By

Zhe Huang

A REPORT

Submitted in partial fulfillment of the requirements for the degree of

MASTER OF SCIENCE

In Electrical Engineering

MICHIGAN TECHNOLOGICAL UNIVERSITY

2014

© 2014 Zhe Huang

This report has been approved in partial fulfillment of the requirements for the Degree of MASTER OF SCIENCE in Electrical Engineering.

Department of Electrical and Computer Engineering

Report Advisor: *Wayne W. Weaver*

Committee Member: *Mahdi Shahbakhti*

Committee Member: *Saeid Nooshabadi*

Department Chair: *Daniel R. Fuhrmann*

Table of Contents

List of Figures ..... **vi**

List of Tables ..... **viii**

Abstract ..... **ix**

1 Introduction **1**
1.1 Introduction of alternating current (AC) motor 1
1.2 The control strategy for AC Motor 2
1.2.1 Scalar control (V/Hz control) 2
1.2.2 Vector control (Field Oriented Control) 3
1.3 Space vector modulation 4
1.4 Voltage source inverter 4

2 Sinusoidal Pulse Width Modulation **6**
2.1 Theory of PWM 6
2.2 Instruction of sinusoidal PWM 7
2.3 Principle of sinusoidal PWM 7
2.4 Modulation index 8

3 Space Vector Pulse Width Modulation **9**
3.1 Rotating Transformation 10
3.2 Principle of SVPWM 13
3.3 Implementation procedure of SVPWM 15
3.3.1 Determine time duration $T1, T2\ and\ T0$ at sector 1 16
3.3.2 Determine the sector of voltage space vector 17
3.3.3 Determine the time duration at any sector 18
3.3.4 Determine the switching time at each sectors 18

4 Z-Source Network Inverter **21**
4.1 Z-source network 21
4.2 Z-source inverter operation principle 22
4.3 Z-source circuit analysis 24

5 Simulation Model **25**
5.1 Model building of hardware circuit 25
5.2 Model building of SVPWM signal generator 27
5.3 Model building of Z-source inverter with modified SVPWM 32

6 Simulation Results **33**
6.1 The SPWM simulation results 33
6.2 The SVPWM simulation results 35
6.3 The Z-source inverter with SVPWM control simulation results 38

7 Conclusion **42**

8 References **43**

List of Figures

Fig. 1.1 (a) AC induction motor; (b) Permanent magnet synchronous motor

Fig. 1.2 Main control methods for AC motor

Fig. 1.3 Stator voltage versus frequency profile under V/Hz Control

Fig. 1.4 Basic Scheme of FOC for AC motor

Fig. 1.5 Traditional two-stage power inverter for HEV applications

Fig. 1.6 The signal of dead band time control for the full bridge inverter

Fig. 2.1 An ideal circuit for generate PWM signal

Fig. 2.2 Voltages in a PWM circuit

Fig. 2.3 Circuit model of three-phase inverter

Fig. 2.4 Control signal generator for SPWM

Fig. 2.5 SPWM signal produce: reference voltage and carrier wave vs. output voltage

Fig. 3.1 Voltage space vector and its component in the αβ stationary reference frame

Fig. 3.2 Park transformation from three-phase to rotating dq0 coordinate system

Fig. 3.3 Three-phase voltage source circuit

Fig. 3.4 Under-modulation regions in space vector representation

Fig. 3.5 Synthesized vector V_{out} as a combination of adjacent vectors at sector 1

Fig. 3.6 Switching patterns of sector I

Fig. 3.7 SVPWM switching patterns at sector I to VI

Fig. 4.1 Z-source inverter for AC motor applications

Fig. 4.2 Equivalent circuit of the Z-source inverter viewed from the dc link

Fig. 4.3 Equivalent circuit of the Z-source inverter viewed from the dc link when the inverter bridge is in the shoot-through zero state

Fig. 4.4 Equivalent circuit of the Z-source inverter viewed from the dc link when the inverter bridge is in one of the eight non shoot-through switching states

Fig. 4.5 Modified PWM control signal with shoot-through zero states

Fig. 5.1 Simulink model of three-phase full bridge inverter system

Fig. 5.2 The ideal IGBT model

Fig. 5.3 Simulink model of LC filter

Fig. 5.4 SVPWM signal generator

Fig. 5.5 Three-phase sinusoidal signal generator and output waveform

Fig. 5.6 Clarke transformation block and output waveform

Fig. 5.7 Reference angel sector block

Fig. 5.8 $T1\ and\ T2$ duration time calculation block

Fig. 5.9 Space vector modulation signal generator and the output waveform

Fig. 5.10 PWM signal generator and the comparison waveform

Fig. 5.11 Three-phase inverter with Z-source network

Fig. 5.12 Additional pulse signal inject into the SPWM/SVPWM signal and work together

Fig. 6.1 SPWM control signal to one phase switches (upper and lower switches)

Fig. 6.2 Output voltage (a) and current (b) of SPWM after LC filter

Fig. 6.3 FFT analysis of SPWM when MI = 0.8

Fig. 6.4 (a) Modulation index vs THD; (b) Modulation index vs output voltage

Fig. 6.5 SVPWM control signal to one phase switches (upper and lower switches)

Fig. 6.6 Output voltage and current of SVPWM after LC filter

Fig. 6.7 FFT analysis of SVPWM when MI = 0.8

Fig. 6.8 (a) Modulation index vs THD; (b) Modulation index vs output voltage

Fig. 6.9 Insert PWM sequence to the SVPWM signal and get the shoot-through time

Fig. 6.10 Output voltage (a) and current (b) of Z-source inverter with modified SVPWM control

Fig. 6.11 FFT analysis of Z-source inverter with shoot-through time control

Fig. 6.12 (a) Frequency vs THD; (b) Frequency vs output voltage

Fig. 6.13 (a) Frequency vs THD; (b) Frequency vs output voltage

Fig. 6.14 (a) Frequency vs THD; (b) Frequency vs output voltage

List of Tables

Table 1 Switches' state and output pole voltage

Table 2 The relationship between switching status and voltage space vector

Table 3 The corresponding relationship between N and sector

Table 4 The effect time of T1、T2、T0 every sector

Table 5 The switching time of T_{cmp1}, T_{cmp2} and T_{cmp3} at each sector

Table 6 Initial system parameters setup

Table 7 Output Voltages and THDs under different modulation index

Table 8 Initial system parameters setup

Table 9 Output Voltages and THDs under different modulation index

Table 10 Initial system parameters setup

Table 11 Output Voltages and THDs with different frequency PWM inserted when MI=0.8, duty cycle = 30%.

Table 12 Output Voltages and THDs with PWM inserted when duty cycle = 30% under different modulation index

Table 13 Output Voltages and THDs under different duty cycle of PWM inserted when *f=4000, MI=1*

Abstract

The voltage source inverter (VSI) and current voltage source inverter (CSI) are widely used in industrial application. But the traditional VSIs and CSIs have one common problem: can't boost or buck the voltage come from battery, which make them impossible to be used alone in Hybrid Electric Vehicle (HEV/EV) motor drive application, other issue is the traditional inverter need to add the dead-band time into the control sequence, but it will cause the output waveform distortion.

This report presents an impedance source (Z-source network) topology to overcome these problems, it can use one stage instead of two stages (VSI or CSI + boost converter) to buck/boost the voltage come from battery in inverter system. Therefore, the Z-source topology hardware design can reduce switching element, entire system size and weight, minimize the system cost and increase the system efficiency. Also, a modified space vector pulse-width modulation (SVPWM) control method has been selected with the Z-source network together to achieve the best efficiency and lower total harmonic distortion (THD) at different modulation indexes. Finally, the Z-source inverter controlling will modulate under two control sequences: sinusoidal pulse width modulation (SPWM) and SVPWM, and their output voltage, ripple and THD will be compared.

Index Terms – VSI, CSI, buck/boost, Z-source, SPWM, SVPWM, ripple, THD.

1 Introduction

1.1 Introduction of alternating current (AC) motor

Since 1822, the first rotating device invented by Englishman *Peter Barlow* [1], with the increasing demand for industry, there are many types electric motor have been invent: AC induction motor (ACIM), brushed direct current (DC) motor, brushless dc motor (BLDC), permanent magnet synchronous motor (PMSM), stepper motor, switched reluctance motor, etc. Due to the alternating current (AC) electric motor does not have a brush or slip-rings structure like a brushed dc motor, so the ac motor does not have all the problems associated with sparking; such as electrical noise, brush wear, high friction, and poor reliability. On the other hand, ac motor is very economical to manufacture and very low maintenance compare with brush dc motor. Without a doubt, the ac motor was become most popular used motor in the industrial and consumer applications, also widely used in the automotive fields.

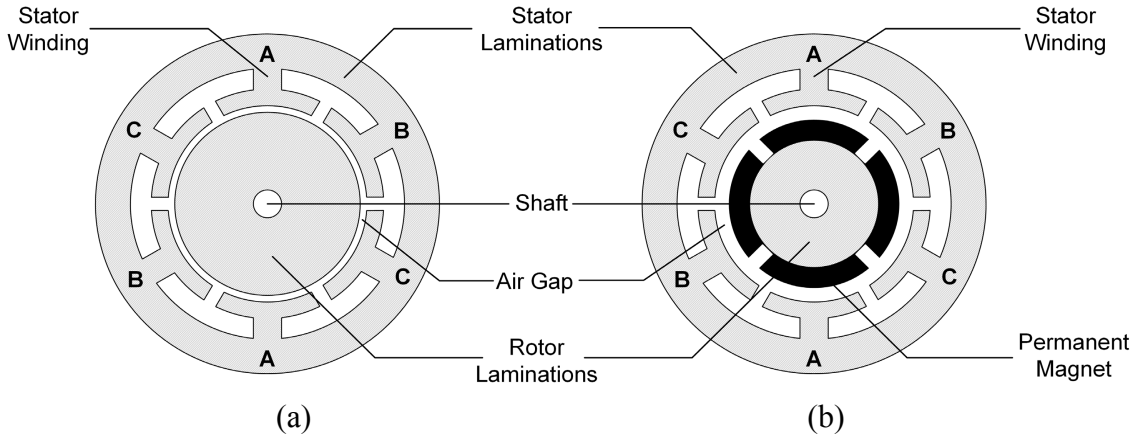

Fig. 1.1 (a) AC induction motor; (b) Permanent magnet synchronous motor

There are two main types of ac motor, the first type is ACIM and the second type is PMSM.

- ***ACIM*** or ***asynchronous motor*** is the most efficient motor where efficiency can achieve 97% or more in high power applications [2]. However, the stator current will be consumed large portion energy to produce the rotor flux when ACIM under low load conditions, so the efficiency will be reduced.

- ***PMSM*** or ***synchronous motor*** provide higher power density pre unit size, it mean that to provide same horsepower, PMSM have smaller size compared to ACIM. It's because the rotor flux is already established in a PMSM by the permanent magnets [3].

Both of ACIM and PMSM have a similar stator structure, where the windings are constructed in such a way as to produce a rotating magnetic field (sinusoidal flux) in the air gap of the machine. Therefore, they work well when driven by sinusoidal waveforms, it mean that ac motor is more difficult to control than brushed dc motor, because the dc motor's RPM have a directly proportional relationship to voltage and a chopper PWM control circuit can easily achieve the speed control. Unlike dc motor, almost ac motors have being used with variable frequency drive (VFD) or inverter to control. VFDs or inverter can offer suitable sinusoidal voltages and sinusoidal currents for ac motors to run, also can adjust the amplitude and frequency of sinusoidal voltage for speed and torque control.

1.2 The control strategy for AC Motor

The ac motor become the most popular motor in the industrial application is because their higher reliability, higher efficiency, very economical to manufacture and low maintenance. However, there are lots of challenging for using ac motors due to their non-linear behavior, their complex mathematical model and the electrical parameter oscillation, which physical parameters will be changed when the temperature changed. Therefore, these problems make the control of ac motor complex and have to use of high performance algorithms to figure out. Due to the rapid development of semiconductor during last decades, the microcontroller already can execute high performance algorithm and also used in the ac motor control fields. Normally, ac drive controls can be technically divided into two types: scalar control and vector control [4].

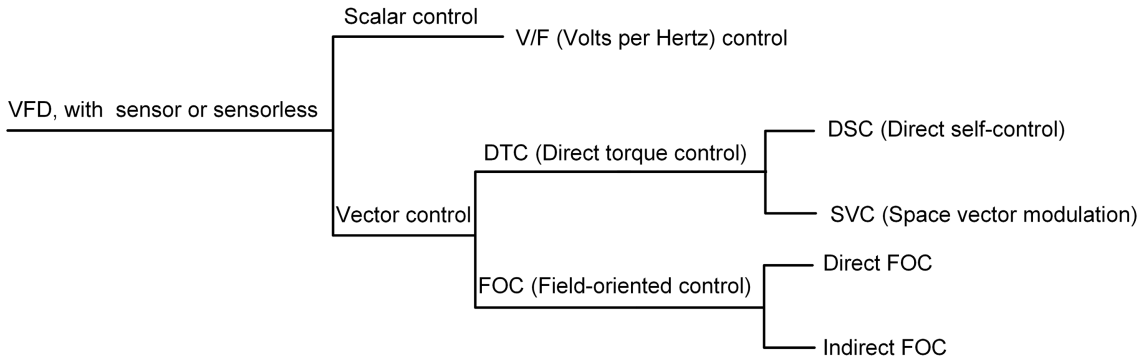

Fig. 1.2 Main control methods for AC motor

1.2.1 Scalar control (V/Hz control)

In the scalar control (V/Hz control), the speed of ac motor can be controlled by increasing or decreasing the voltage and frequency that supply to the stator that air gap flux is always kept at the desired value at the steady-state. If the stator voltage increases or frequency decreases, the coils can be burned or got saturation. To avoid these issues happen, the stator

voltage and frequency should be changed at the same time. Other disadvantage of V/Hz control is that control of torque is not possible [5].

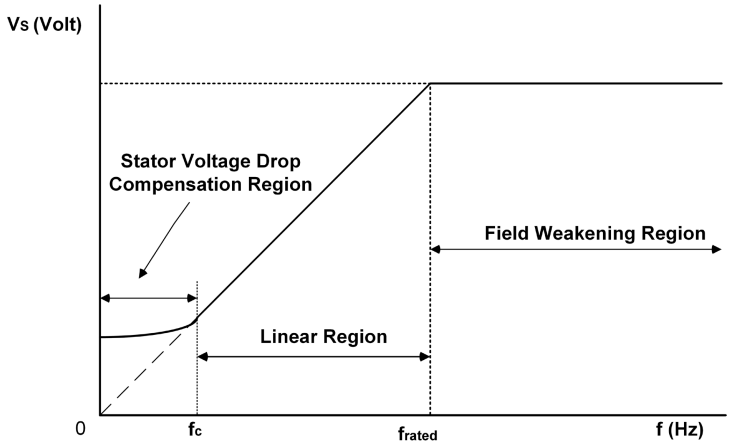

Fig. 1.3 Stator voltage versus frequency profile under V/Hz Control

1.2.2 Vector control (Field Oriented Control)

Due to V/Hz control has some natural limitations on the performance, engineers need to find other way to solve these problems and achieve high dynamic performance for ac motor control. In the early 1970s, a more complex control method: field-oriented control (FOC also called vector control) had proposed by *K. Hasse* and *Siemens' F. Blaschke* at Technical University Darmstadt. After that, Technical University Braunschweig's *Werner Leonhard* [6] developed the Field Oriented Control (FOC) techniques and made it possible can be used in the ac drives.

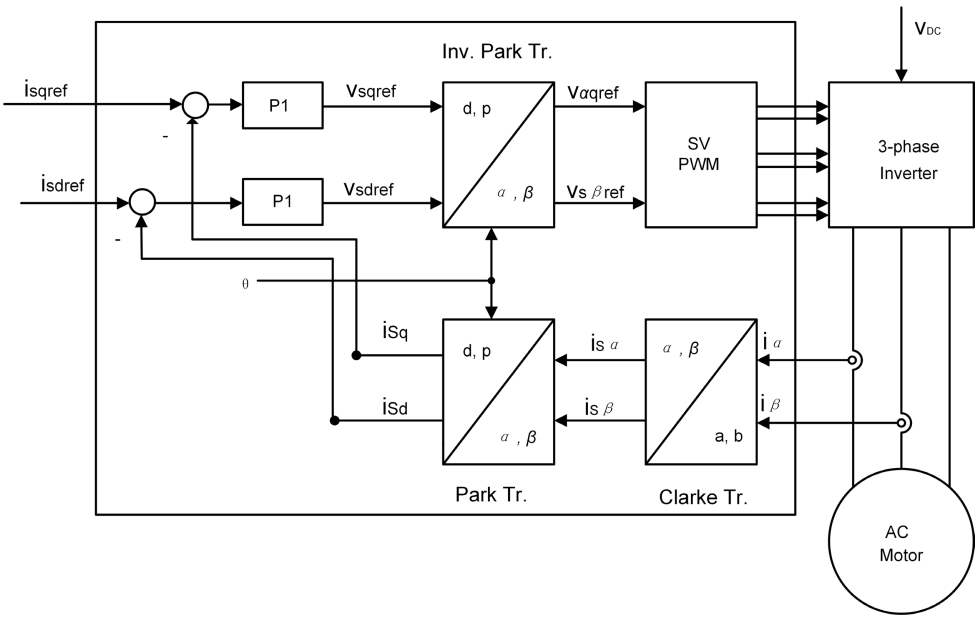

Fig. 1.4 Basic Scheme of FOC for AC motor

In order to simply control the AC motor, FOC algorithm allows engineer to separately control the torque and the magnetizing flux. From Fig. 1.4, we can see the whole FOC controlling system just need two constants: the torque component (i_{Sq}) and the flux component (i_{Sd}) as its input references. Therefore, the FOC algorithm made the AC motor control more easier like DC machine control [7], because of there are only two components need to control by PI controller in the FOC machines. To decouple the torque and flux, it is need to use several mathematical transforms to calculate the result. It is a big challenge for microcontroller to processing the FOC algorithm until the high performance microcontroller come out and used in the industry. This means that mathematical transformations can be carried out very quickly by the microcontrollers, and the motor controlling can be executed at a fast rate to achieve higher dynamic performance.

1.3 Space vector modulation

From the Fig. 1.4, we know the FOC controlling system is consist of three mainly parts: mathematical transformations (Clarke transformation and Park transformation), pulse width modulation (PWM) generator and proportional-integral-derivative controller (PID controller). Compare with other PWM technique, space vector pulse width modulation (SVPWM or SVM) has become the most important PWM technique for the 3-phase voltage source inverter or current source inverter (VSI or CSI). This report focuses on a modified SVPWM technique for Z-source inverter. The reason of choice SVPWM is because of some advantages shown below:

- High utilization from DC bus (15.5% higher output voltage compared to SPWM)
- Lower switching losses
- Less total harmonic distortion (THD)

1.4 Voltage source inverter

The commonly inverters/converters can be classified as voltage source (VS) and current source (CS) inverter (or converter which depending on the power flow directions). Normally, a dc voltage source inverter will be paralleled with a large capacitor as the input, and a dc current source inverter will added a large inductor.

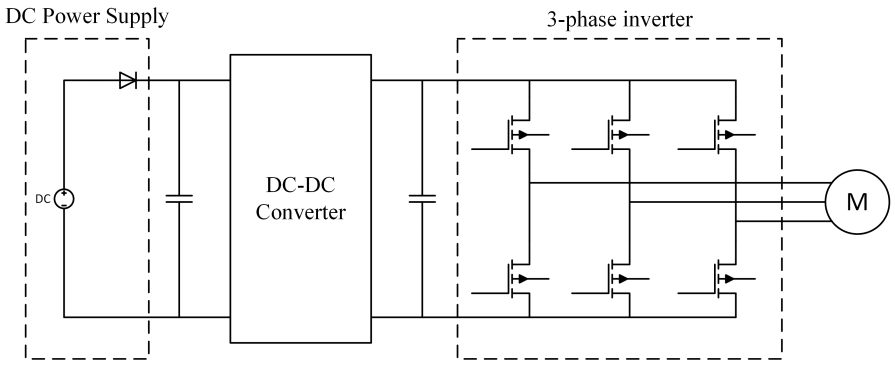

Fig. 1.5 Traditional two-stage power inverter for HEV applications

The VSI is widely used in the VFD, uninterrupted power supply (UPS), and solar energy applications. However, it has the following natural limitations [8]:

- The ac output voltage cannot exceed dc input voltage, therefore all the VSI is a buck inverter and it needed an additional dc-dc boost converter to obtain a desired ac output voltage. Meanwhile, the additional boost converter will increase the total cost and size of system.

- Need a dead band time (dead band is an interval of a signal domain or band where no action occurs) control to the inverter. From Fig. 1.5 shows the traditional 3-phase power inverter structure, we know the upper and lower switches of each phase leg cannot open at the same time, otherwise the shoot-through problem will cause the short circuit and system will be damaged. To avoid it happen, dead band time control (Fig. 1.6) will be added to the SVPWM control, however when add the dead band to the control signal will causes the output waveform distortion.

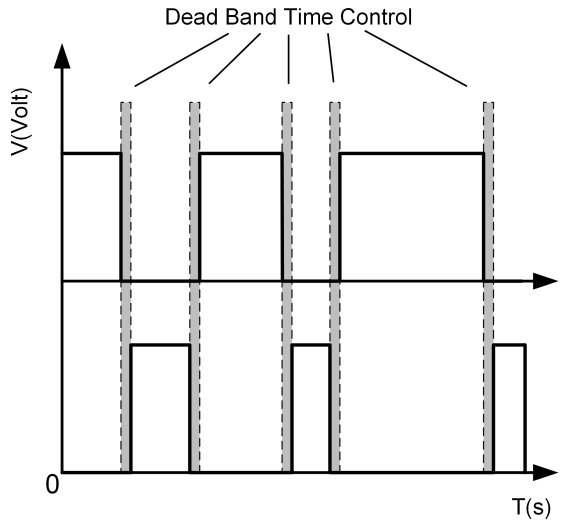

Fig. 1.6 The signal of dead band time control for the full bridge inverter

2 Sinusoidal Pulse Width Modulation

2.1 Theory of PWM

Pulse-width modulation (PWM) technique is a method to generate variable voltage magnitudes and difference forms by control the pulse duration in every full period. The basic idea is shown in the following figures.

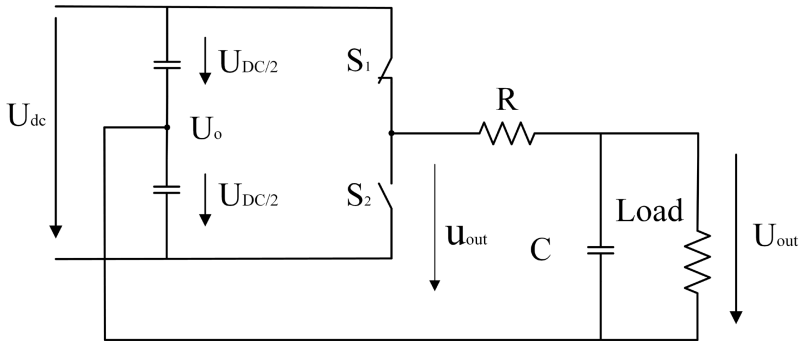

Fig. 2.1 An ideal circuit for generate PWM signal

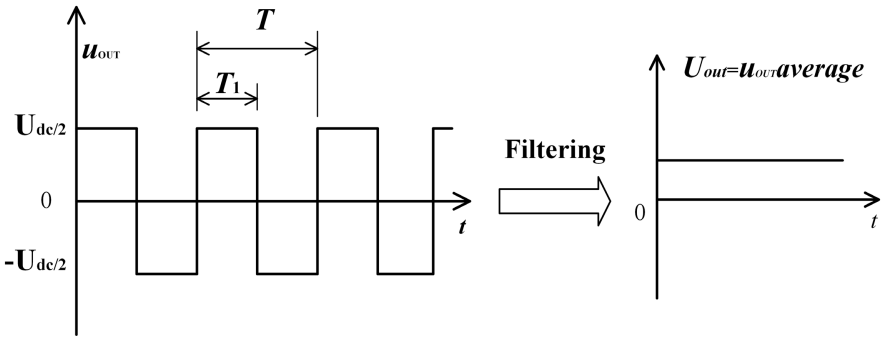

Fig. 2.2 Voltages in a PWM circuit

In Fig. 2.1 shows circuit, the input voltage is constant and which value is U_{dc}. Assume the PWM signal has a constant period T, switch S_1 turned on and S_2 turned off during time T_1, so the switch state is reversed in the rest of the period $T_2 = T - T_1$. If let the PWM output pass an ideal filter (assume no energy loss), so the output dc voltage will be

$$U_{out} = (\frac{T_1}{T} - \frac{1}{2}) \times U_{dc} \quad (1)$$

From formula (1), we know the output voltage has a linear relationship with duty cycle (T_1/T), so the output voltage (shows in Fig. 2.2) can be increased or decreased by change the duty cycle in all the PWM application [10].

2.2 Instruction of sinusoidal PWM

Since PWM technique appeared in the world, the carrier-based PWM methods were widely used and developed in the communication technology and power control fields. SPWM technique is one of the earliest modulation signals for carrier-based PWM, the main idea of SPWM is using sinusoidal modulation signal compare with a carrier signal (normally is ramp wave) to produce. The on/off duration time of the six switches in the inverter system (Fig. 2.3) is depending on the intersections between the reference waveform (sinusoidal wave) and the carrier waveform. SPWM control for inverter is very easy to achieve and just need a low cost microcontroller, however, SPWM is unable to fully utilize the dc bus voltage and the dc bus utilization rate is only 78.5%.

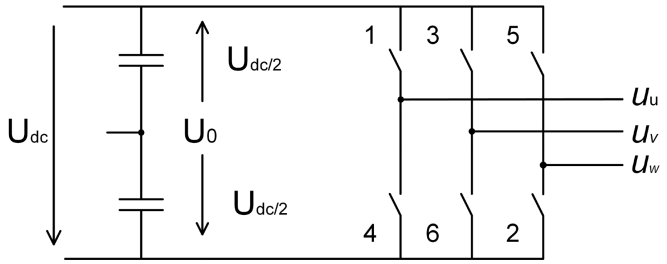

Fig. 2.3 Circuit model of three-phase inverter

2.3 Principle of sinusoidal PWM

The Fig. 2.4 shows a control signal generator for sinusoidal PWM, we use the 60 Hz three sinusoidal waves (V_u, V_v, V_w) which is lagging or leading other phase 120° to compare with a high frequency (5000Hz) triangular waveform (V_T).

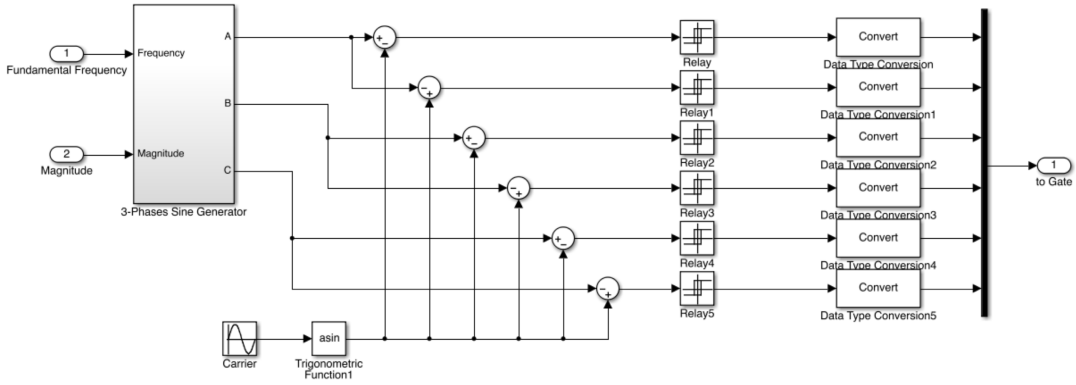

Fig. 2.4 Control signal generator for SPWM

The three phase outputs will be connected to the middle of each bridge as shown in Fig. 2.3, when the upper switch open, the lower switches will close and vice-versa. Assume the

DC voltage is cascade by two DC voltage power and each value is $V_{DC}/2$, so in this circuit, the voltage of output pole V_{uo}, V_{vo}, V_{wo} will switch between $V_{DC}/2\ and\ -V_{DC}/2$ which depending on the upper and lower switches on/off states.

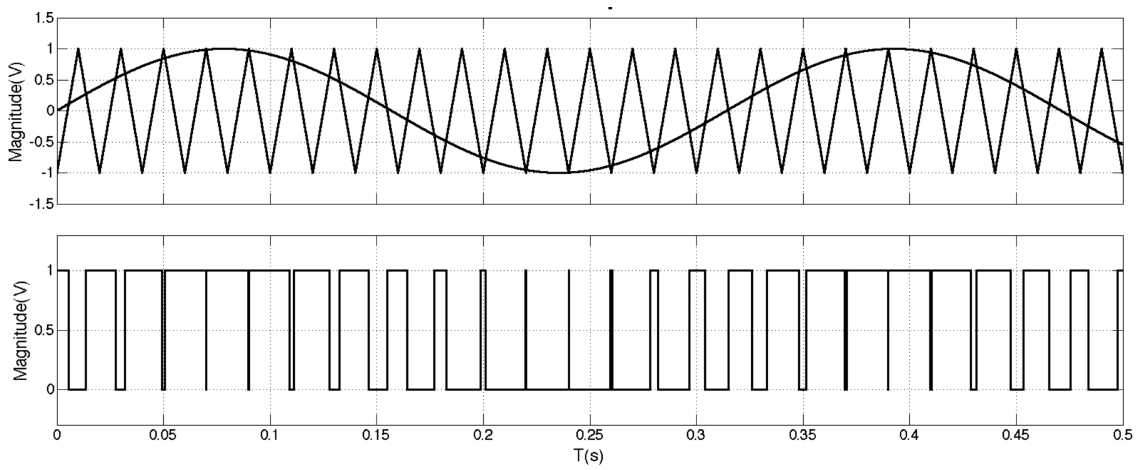

Fig. 2.5 SPWM signal produce: reference voltage and carrier wave vs. output voltage

Base on the principle of SPWM shown as Fig. 2.4, the sinusoidal wave compared with high frequency triangular wave and the inverter output voltage is determined in the following table:

Table 1 Switches' state and output pole voltage

Switch On	Sinusoidal wave vs. triangular wave	Output pole voltage
S_1	$V_u > V_T$	$V_{uo} = 0.5V_{dc}$
S_3	$V_v > V_T$	$V_{vo} = 0.5V_{dc}$
S_5	$V_w > V_T$	$V_{wo} = 0.5V_{dc}$
S_4	$V_u < V_T$	$V_{uo} = -0.5V_{dc}$
S_6	$V_v < V_T$	$V_{vo} = -0.5V_{dc}$
S_2	$V_w < V_T$	$V_{wo} = -0.5V_{dc}$

The line-to-line output voltages is based on the pole voltages:

$$\begin{cases} V_{uv} = V_{uo} - V_{vo} \\ V_{vw} = V_{vo} - V_{wo} \\ V_{wu} = V_{wo} - V_{uo} \end{cases} \quad (2)$$

2.4 Modulation index

Fig 2.2 shows the square wave has a magnitude $U_{dc}/2$ and its frequency is $f = 1/T$, using Fourier expansion we can represent as:

$$x_{square} = \frac{4}{\pi}(sin(2\pi ft) + \frac{1}{3}sin(2\pi ft) + \frac{1}{5}sin(10\pi ft) + \cdots) \quad (3)$$

So the first item of the square wave in Fourier expansion is

$$\frac{4}{\pi} \times \frac{U_{dc}}{2} = 2U_{dc}/\pi \quad (4)$$

Therefore, the magnitude of the output voltage can be adjusted by change the magnitude of reference signal, the concept shown in Fig 2.6. The maximum modulation index concept is used to calculate the ability of a SPWM to produce AC voltage [11]:

$$m_{SPWM} = \frac{U_{PWM}}{U_{reference}} = \frac{U_{dc}/2}{2U_{dc}/\pi} = \frac{\pi}{4} \approx 0.7855 = 78.55\% \quad (5)$$

The modulation index is defined as formula (5), where U_{PWM} is the value of maximum SPWM output voltage ($U_{dc}/2$) and $U_{reference}$ is the first item of Fourier series of a square wave.

3 Space Vector Pulse Width Modulation

Space vector PWM (SVPWM) is a technique designed for three phase ac motor inverter control, it work depending on their special switching sequence and effect of combination of different pulse width. As a result, the windings in the ac motor will generate the three-phase sinusoidal waves which have 120° phase shifts and less harmonics. Compare with SPWM, SVPWM have three main advantages:

- Higher dc voltage utilization
- Higher fundamental component and less harmonics
- SVPWM is better control the ac motor by digital control system

3.1 Rotating Transformation

The performance of three-phase motor is described by their voltage equations. Let U_m as the peak value of three-phase sinusoidal voltage and $\omega = 2\pi f$ is the radian frequency, so the three-phase sinusoidal mathematical system can be represented:

$$\begin{aligned} u_a &= U_m cos\omega t \\ u_b &= U_m \cos(\omega t - \tfrac{2}{3}\pi) \\ u_c &= U_m cos(\omega t + \tfrac{2}{3}\pi) \end{aligned} \tag{6}$$

Transform three-phase domain to two-phase domain (stationary coordinate system) by using $\alpha\beta$ components:

$$\begin{aligned} u_a &= U_m \cos\omega t \\ &= U_\alpha \\ u_b &= U_m \cos(\omega t - 120^\circ) \\ &= U_\alpha \cos 120^\circ + U_\beta \sin 120^\circ \\ &= -\frac{1}{2}U_\alpha + \frac{\sqrt{3}}{2}U_\beta \\ u_c &= U_m \cos(\omega t + 120^\circ) \\ &= U_\alpha \cos 120^\circ - U_\beta \sin 120^\circ \\ &= -\frac{1}{2}U_\alpha - \frac{\sqrt{3}}{2}U_\beta \end{aligned} \tag{7}$$

Let the equations (7) rewrite as matrixes, and we get *Clarke inverse transformation* [12]:

$$\begin{pmatrix} u_a \\ u_b \\ u_c \end{pmatrix} = \begin{pmatrix} 1 & 0 \\ -1/2 & \sqrt{3}/2 \\ -1/2 & -\sqrt{3}/2 \end{pmatrix} \begin{pmatrix} U_\alpha \\ U_\beta \end{pmatrix} \tag{8}$$

Then exchange $\alpha\beta$ items and *abc* items from matrix (8):

$$\begin{pmatrix} U_\alpha \\ U_\beta \end{pmatrix} = P \begin{pmatrix} u_a \\ u_b \\ u_c \end{pmatrix} \tag{9}$$

So the *P* matrix can be written: (*Clark transformation or* $\alpha - \beta$ *transformation*)

$$P = \frac{2}{3}\begin{pmatrix} 1 & -1/2 & -1/2 \\ 0 & \sqrt{3}/2 & -\sqrt{3}/2 \end{pmatrix} \tag{10}$$

Fig. 3.1 shows the voltage vectors of $[U_a, U_b, U_c]$, there is a complex plane and the real axis is overlap with the *a*-axis.

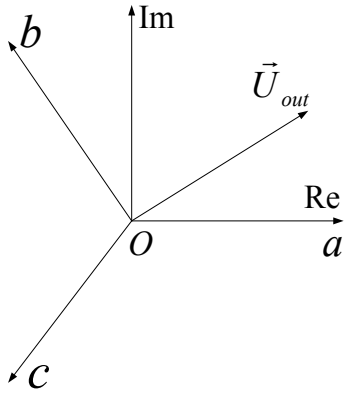

Fig. 3.1 Voltage space vector and its component in the $\alpha\beta$ stationary reference frame

From the *Clarke transformation* we can derivate the *Park transformation* (*dp0 transform*):

$$\begin{aligned} u_d cos\theta + u_q sin\theta &= u_\alpha \\ u_d sin\theta - u_q cos\theta &= u_\beta \end{aligned} \tag{11}$$

$$\begin{pmatrix} u_\alpha \\ u_\beta \end{pmatrix} = \begin{pmatrix} cos\theta & sin\theta \\ sin\theta & -cos\theta \end{pmatrix} \begin{pmatrix} u_d \\ u_q \end{pmatrix} \tag{12}$$

Let equations (11) multiply by $cos\theta \; and \; sin\theta$:

$$\begin{aligned} u_d cos^2\theta + u_q sin\theta cos\theta &= u_\alpha cos\theta \\ u_d sin^2\theta - u_q sin\theta cos\theta &= u_\beta sin\theta \end{aligned} \tag{13}$$

Then accumulate two equations in the (13), we can get

$$u_d = u_\alpha cos\theta + u_\beta sin\theta \tag{14}$$

Let equations (11) multiply by $sin\theta \; and \; cos\theta$:

$$\begin{aligned} u_d sin\theta cos\theta + u_q sin^2\theta &= u_\alpha sin\theta \\ u_d sin\theta cos\theta - u_q cos^2\theta &= u_\beta cos\theta \end{aligned} \tag{15}$$

Similarly, accumulate two equations in the (15):

$$u_q = u_\alpha sin\theta - u_\beta cos\theta \tag{16}$$

And merger equation (14) and (16):

$$\begin{pmatrix} u_d \\ u_q \end{pmatrix} = \begin{pmatrix} cos\theta & sin\theta \\ sin\theta & -cos\theta \end{pmatrix} \begin{pmatrix} u_\alpha \\ u_\beta \end{pmatrix} \tag{17}$$

Finally, we get *Park transformation (dq0 transformation):*

$$\begin{pmatrix} u_d \\ u_q \end{pmatrix} = \frac{2}{3} \begin{pmatrix} \cos\theta & \cos(\theta - 120^\circ) & \cos(\theta + 120^\circ) \\ \sin\theta & \sin(\theta - 120^\circ) & \sin(\theta + 120^\circ) \end{pmatrix} \begin{pmatrix} u_a \\ u_b \\ u_c \end{pmatrix} \tag{18}$$

And the *Park inverse transformation* is:

$$K_s{}^{-1} = \begin{pmatrix} cos(\theta) & sin(\theta) \\ cos(\theta - 120^\circ) & sin(\theta - 120^\circ) \\ cos(\theta + 120^\circ) & sin(\theta + 120^\circ) \end{pmatrix} \tag{19}$$

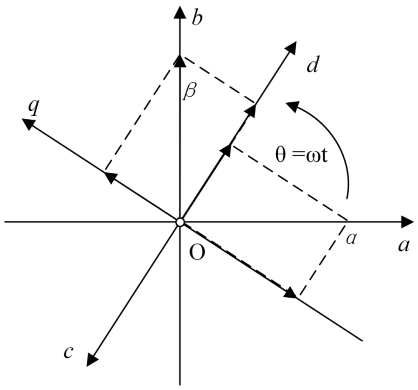

Fig. 3.2 *Park transformation* from three-phase to rotating dq0 coordinate system

The essential of Park transformation can be seen as an extension of the Clarke transformation, convert a stationary reference frame to a synchronously rotating reference frame by using a mathematical transformation. Due to we convert abc frame to dq0 frame, two phase voltage now turn into dc quantity (time-invariant). Because of d-flux component and q-torque component can be controlled independently and the reference frame rotates with the electrical frequency, therefore, the torque control becomes easier than original three-phase system.

3.2 Principle of SVPWM

The three-phase voltage source inverter basic circuit shows in the Fig. 3.3. Let's say the six letters a, b, c and a', b', c' represent the status of six switches in this circuit. When a, b and c equal to 1, it mean that upper switches open in the inverter, at the same time, the lower switches close and a', b', c' equal to 0; vice versa, the upper switches close and a, b and c equal to 0. Therefore, the three-phase inverter controlled by six switches that have eight configurations.

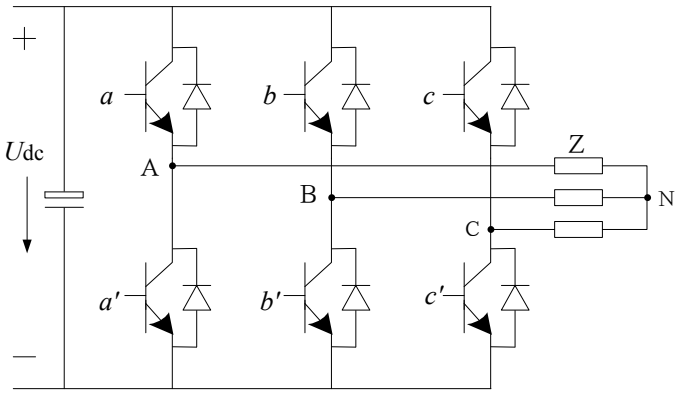

Fig. 3.3 Three-phase voltage source circuit

Base on the eight switching statuses in the inverter, there are eight different voltage space vectors and can be represent by one formula:

$$\vec{U}_{\text{out}} = \frac{2U_{\text{dc}}}{3}(a + be^{\text{j}\frac{2}{3}\pi} + ce^{-\text{j}\frac{2}{3}\pi}) \tag{20}$$

The reference voltage vector $\vec{U}_{out}$ will rotates with an angular velocity $\omega = 2\pi f$, where f is the fundamental frequency of the output voltage. The relationship between switching status and voltage space vector is show in Table 2, there are eight different switching statuses within two zero vectors ($\vec{V}_0$ *and* $\vec{V}_7$) and six active vectors ($\vec{V}_1$ *to* $\vec{V}_6$).

Table 2 The relationship between switching status and voltage space vector

Voltage Vectors	Switching Vectors			Line to neutral voltage			Output voltage
	a	**b**	**c**	V_{an}	V_{bn}	V_{cn}	$\vec{U}_{out}$
V_0	0	0	0	0	0	0	0
V_1	1	0	0	$2U_{\text{dc}}/3$	$-U_{\text{dc}}/3$	$-U_{\text{dc}}/3$	$\frac{2}{3}U_{\text{dc}}$
V_2	0	1	0	$-U_{\text{dc}}/3$	$2U_{\text{dc}}/3$	$-U_{\text{dc}}/3$	$\frac{2}{3}U_{dc}e^{j\frac{2\pi}{3}}$
V_3	1	1	0	$U_{\text{dc}}/3$	$U_{\text{dc}}/3$	$-2U_{\text{dc}}/3$	$\frac{2}{3}U_{dc}e^{j\frac{\pi}{3}}$
V_4	0	0	1	$-U_{\text{dc}}/3$	$-U_{\text{dc}}/3$	$2U_{\text{dc}}/3$	$\frac{2}{3}U_{dc}e^{j\frac{4\pi}{3}}$
V_5	1	0	1	$U_{\text{dc}}/3$	$-2U_{\text{dc}}/3$	$U_{\text{dc}}/3$	$\frac{2}{3}U_{dc}e^{j\frac{5\pi}{3}}$
V_6	0	1	1	$-2U_{\text{dc}}/3$	$U_{\text{dc}}/3$	$U_{\text{dc}}/3$	$\frac{2}{3}U_{dc}e^{j\pi}$
V_7	1	1	1	0	0	0	0

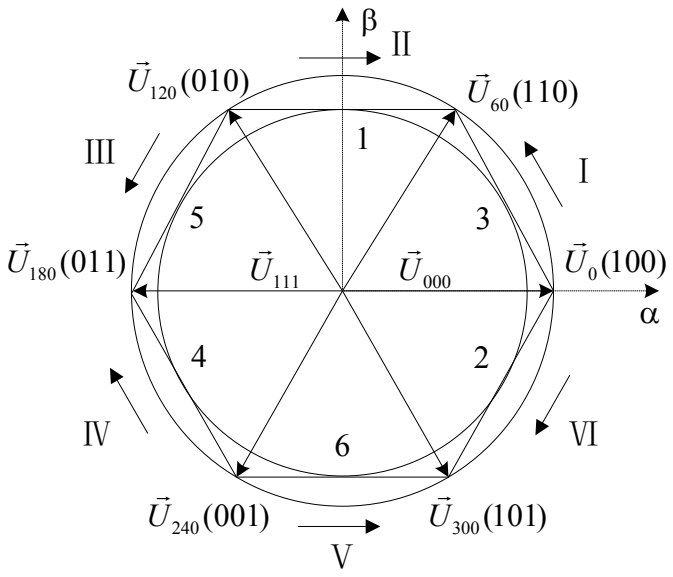

Fig. 3.4 Under-modulation regions in space vector representation

In the normally SVPWM application, we just using six active vectors, but the next chapter will introduce how to use the zero vector $\vec{V}_7$ to produce the shoot-through time in the inverter.

3.3 Implementation procedure of SVPWM

The implementation of SVPWM algorithm is change the average value of voltage on the load by turning the switches on/off time, and let the average voltage equal to synthesized vector voltage $\vec{U}_{out}$. The entire space has been divided into six same sectors of 60° apart in Fig. 3.4, each of them split by two active vector ($\vec{V}_1 \; to \; \vec{V}_6$). The other zero vectors ($\vec{V}_0 \; and \; \vec{V}_7$) with zero amplitude located at the origin of the hexagon.

Assume $\vec{U}_{out}$ is belong to voltage vector *K* region in some time, so the vector voltage $\vec{U}_{out}$ is synthesized by two adjacent active vectors $\vec{U}_K$, $\vec{U}_{K+1}$ and one zero vector $\vec{U}_0$. In this sector, $\vec{U}_K$ is named primary active vector and $\vec{U}_{K+1}$ is named secondary active vector, and $\vec{U}_K$, $\vec{U}_{K+1}$ action time are $T_K \; and \; T_{K+1}$, zero vector $\vec{U}_0$ action time is T_0. In order to explain how to generate the synthesized vector voltage $\vec{U}_{out}$, here is the $T_1, T_2 \; and \; T_0$ calculation of sector 1 and shows in Fig. 3.5.

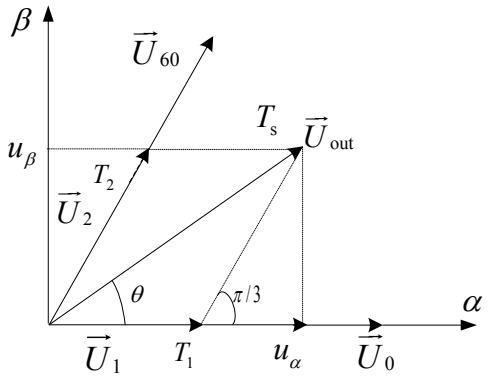

Fig. 3.5 Synthesized vector $\vec{U}_{out}$ as a combination of adjacent vectors at sector 1

3.3.1 Determine time duration T_1, T_2 and T_0 at sector 1

$$T_{\text{PWM}}\vec{U}_{\text{out}} = T_1\vec{U}_0 + T_2\vec{U}_{60} + T_0(\vec{U}_{000} \text{ or } \vec{U}_{111}) \tag{21}$$

Where

$$T_1 + T_2 + T_0 = T_{\text{PWM}} \tag{22}$$

$$\vec{U}_1 = \frac{T_1}{T_{PWM}}\vec{U}_0$$
$$\vec{U}_2 = \frac{T_2}{T_{PWM}}\vec{U}_{60} \tag{23}$$

In equation (23), T_1, T_2 and T_0 are active vectors $\overrightarrow{U_0}$, $\overrightarrow{U_{60}}$ and zero vectors $\overrightarrow{U_{000}}$, $\overrightarrow{U_{111}}$ time duration. From the Fig 3.5, we can get

$$\frac{\left|\vec{U}_{\text{out}}\right|}{\sin 2\pi/3} = \frac{\left|\vec{U}_1\right|}{\sin(\pi/3-\theta)} = \frac{\left|\vec{U}_2\right|}{\sin\theta} \tag{24}$$

Then plugged equation (23) into equation (24), we get

$$T_1 = \sqrt{3}\frac{U_m}{U_{dc}} T_{PWM} \sin\left(\frac{\pi}{3} - \theta\right)$$

$$T_2 = \sqrt{3}\frac{U_m}{U_{dc}} T_{PWM} \sin\theta \tag{25}$$

$$T_0 = T_{PWM}\left(1 - \sqrt{3}\frac{U_m}{U_{dc}}\cos\left(\frac{\pi}{6} - \theta\right)\right)$$

$$\rightarrow\ T_0 = T_{PWM} - T_1 - T_2 \tag{26}$$

3.3.2 Determine the sector of voltage space vector

In order to determine which voltage space vector will be used to generate the synthesized vector voltage $\vec{U}_{out}$, we need to using the value U_α and U_β that in the $\alpha\beta$ coordinate system to determine which sector will work on the active statue. Define three variable values $U_{ref1}, U_{ref2}\ and\ U_{ref3}$ in the equation (27):

$$U_{ref1} = u_\beta$$

$$U_{ref2} = \sqrt{3}u_\alpha - u_\beta \tag{27}$$

$$U_{ref3} = -\sqrt{3}u_\alpha - u_\beta$$

Then define other three variable values *A, B and C*, build the relationship like below:

If $U_{ref1} > 0$, then $A = 1$, otherwise, $A = 0$;

If $U_{ref2} > 0$, then $B = 1$, otherwise, $B = 0$;

If $U_{ref3} > 0$, then $C = 1$, otherwise, $C = 0$.

Let

$$N = 4 \times C + 2 \times B + A \tag{28}$$

then we can get the relationship between N and sector and already shown in the Fig. 3.4:

Table 3 The corresponding relationship between N and sector

N	3	1	5	4	6	2
Sector	I	II	III	IV	V	VI

3.3.3 Determine the time duration at any sector

From Fig. 3.5 we have:

$$u_\alpha = \frac{T_1}{T_{PWM}}|U_0| + \frac{T_2}{T_{PWM}}|U_{60}|\cos\frac{\pi}{3}$$

$$u_\beta = \frac{T_2}{T_{PWM}}|U_{60}|\sin\frac{\pi}{3} \tag{29}$$

Then

$$T_1 = \frac{\sqrt{3}T_{PWM}}{2U_{dc}}\left(\sqrt{3}u_\alpha - u_\beta\right)$$

$$T_2 = \frac{\sqrt{3}T_{PWM}}{U_{dc}}u_\beta \tag{30}$$

After analyze the formula (29), we get the time duration at other sector

$$\mathrm{X} = \frac{\sqrt{3}T_{PWM}u_\beta}{U_{dc}}$$

$$\mathrm{Y} = \frac{\sqrt{3}T_{PWM}}{U_{dc}}\left(\frac{\sqrt{3}}{2}u_\alpha + u_\beta\right)$$

$$\mathrm{Z} = \frac{\sqrt{3}T_{PWM}}{U_{dc}}\left(-\frac{\sqrt{3}}{2}u_\alpha + u_\beta\right) \tag{31}$$

Table 4 The effect time of T1、T2、T0 every sector

N	1	2	3	4	5	6
T_1	Z	Y	-Z	-X	X	-Y
T_2	Y	-X	X	Z	-Y	-Z
T_0	$T_0 = T_{PWM} - T_1 - T_2$					

3.3.4 Determine the switching time at each sectors

The best way to reduce the switching loss is shown in Fig. 3.6: only change one switch bridge statue (0 to 1 or 1 to 0) in each interval from left to right in each sector.

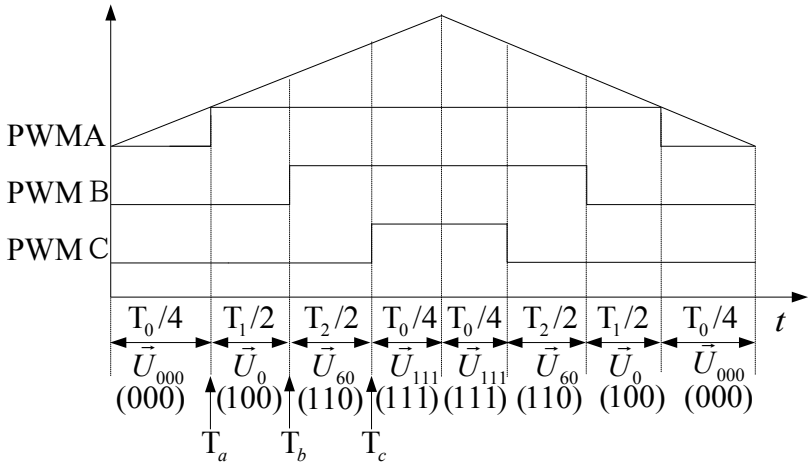

Fig. 3.6 Switching patterns of sector I

Fig. 3.7 shows SVPWM switching patterns at sector I to VI, and the switching time at each sector can be calculated by formula (32). Based on the Fig 3.7 and formula (32), a Simulink model will be built to implement SVPWM.

$$T_a = (T_{PWM} - T_1 - T_2)/4$$
$$T_b = T_a + T_1/2$$
$$T_c = T_b + T_2/2 \quad (32)$$

Table 5 The switching time f T_{cmp1}, T_{cmp2} and T_{cmp3} at each sector

N	1	2	3	4	5	6
T_{cmp1}	T_b	T_a	T_a	T_c	T_c	T_b
T_{cmp2}	T_a	T_c	T_b	T_b	T_a	T_c
T_{cmp3}	T_c	T_b	T_c	T_a	T_b	T_a

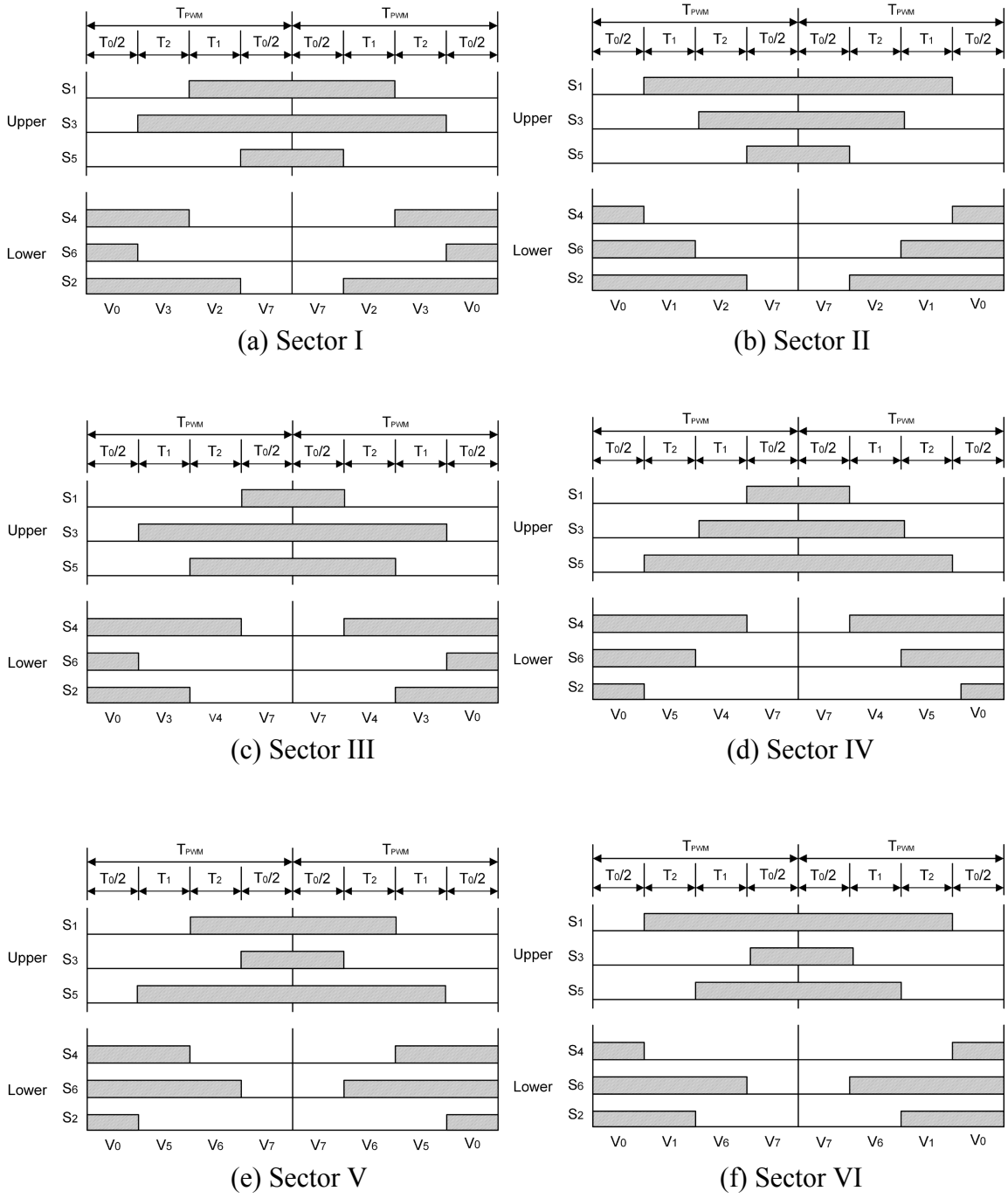

Fig. 3.7 SVPWM switching patterns at sector I to VI

In Fig. 3.6 and Table 5, we know the upper switches open duration time only have T_a, T_b *and* T_c but different combination in the six active sectors, based on this relationship

shown in Fig. 3.6 and Table 5, we can implement six active SVPWM switching patterns in Fig. 3.7.

4 Z-Source Network Inverter

Normally there are two types inverter: VSI and CSI. Both of them are widely used in the VFD, uninterrupted power supply (UPS), and solar energy applications. However, the ac output voltage cannot exceed dc input voltage and the dead band time controlling is needed to add in the VSI or CSI application. Due to this reason, many inverter applications needed an additional dc-dc boost converter to obtain a desired ac output voltage. Meanwhile, if using dead band time control in the inverter system, it will cause the distortion of output waveform; if not using the dead band time control, the shoot-through problem will come out.

4.1 Z-source network

In order to overcome these problems, the Z-source network inverter has been proposed by Dr. *Fangzheng Peng* in 2003 [9]. Fig. 4.1 shows the structure of Z-source inverter, which is made of two capacitors and two inductances, the inductance L_1 and L_2 connected in series and capacitors C_1 and C_2 connected in X shape. Both of them create a two-port impedance network between dc source and three-phase inverter.

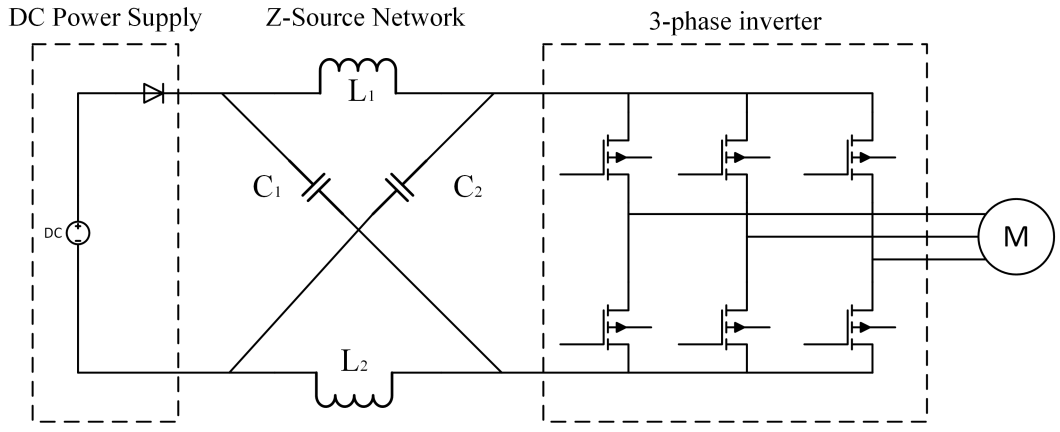

Fig. 4.1 Z-source inverter for AC motor applications

Using shoot-through time to boost output voltage is a unique characteristic in the Z-source circuit. Due to this reason, the Z-source network not only can boost the output voltage

without additional DC-DC converter, but also can generate the AC voltage without dead band time control. Hence, output AC voltage generate by Z-source has less distortion of output waveform, and it can provide more reliability under Electro-Magnetic Interference (EMI) noise.

4.2 Z-source inverter operation principle

Normally, there are eight switching statuses (vector) in the three-phase SVPWM control system, six active statuses and two zero statuses. But there are total nine statuses in Z-source inverter, eight statues is as the same with traditional three-phase inverter and one extra zero status. In this extra zero status, the circuit between inverter and DC source are shorted by upper and lower switches turn on at same time in any one bridge, any two bridges or all bridges.

All the SPWM or SVPWM control pattern can be used in the Z-source inverter because their switching sequence also work in the Z-source inverter without the extra zero status. The figures shown below are the equivalent circuit of Z-source inverter in different states.

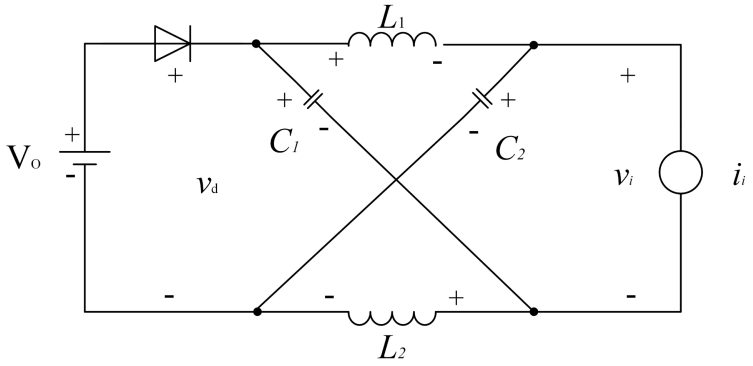

Fig. 4.2 Equivalent circuit of the Z-source inverter viewed from the dc link

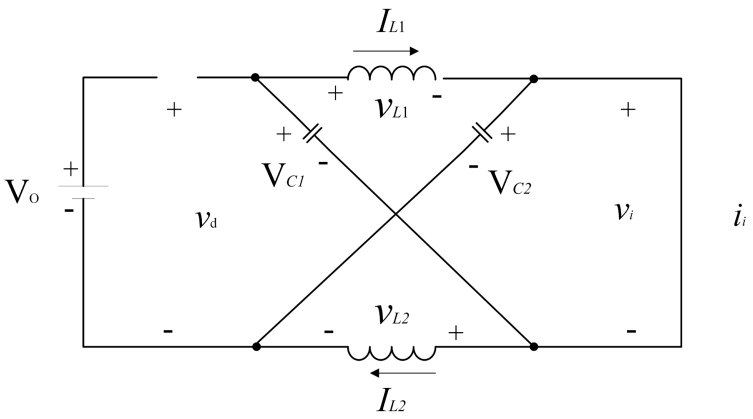

Fig. 4.3 Equivalent circuit of the Z-source inverter viewed from the dc link when the inverter bridge is in the shoot-through zero state

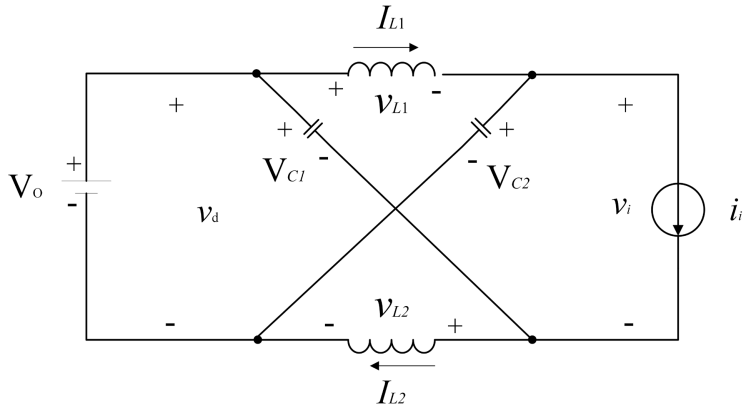

Fig. 4.4 Equivalent circuit of the Z-source inverter viewed from the dc link when the inverter bridge is in one of the eight non shoot-through switching states

A Modified PWM control signal with shoot-through zero states waveform is shown in Fig. 4.5. From this figure, we can observe the PWM switching sequence still does change on the lower switch but the switching sequence on the upper switch become more widely, so that the upper and lower switching will have some time open at the same time. Therefore, the shoot-through time is shown as the overlap part in the Fig. 4.5.

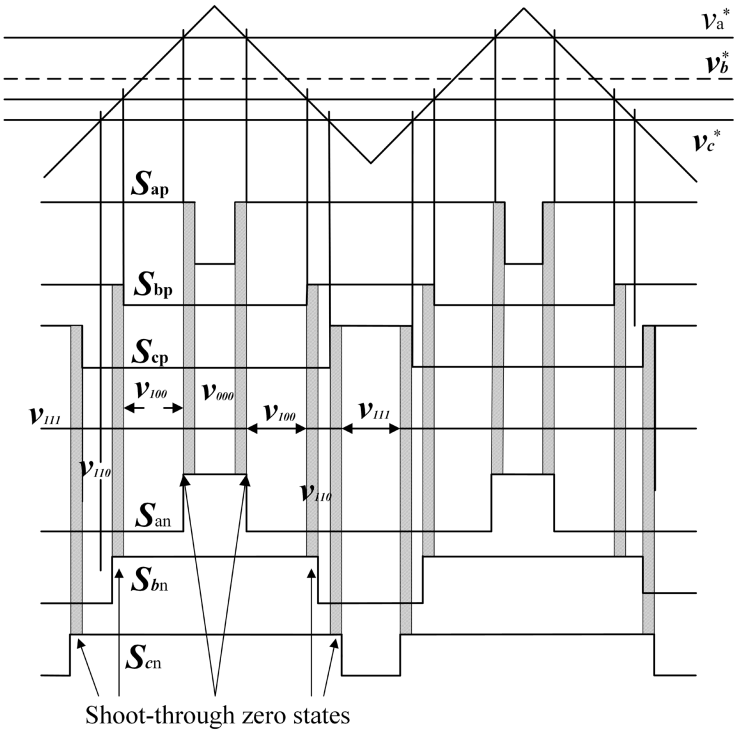

Fig. 4.5 Modified PWM control signal with shoot-through zero states

4.3 Z-source circuit analysis

From Fig. 4.2, we can assume all the inductors L_1, L_2 and capacitors C_1, C_2 have the same value in the Z-Network: $L\ and\ C$. Let

$$V_{C1} = V_{C2} = V_C,\ V_{L1} = V_{L2} = V_L \tag{33}$$

Given that the inverter bridge is in the shoot-through state for an interval of t_0, during a switching cycle, and from the equivalent circuit, one has

$$V_L = V_C, v_d = 2V_C,\ v_i = 0. \tag{34}$$

Set non-shoot-through states for an interval of t_1, in one switching cycle t, we have $t = t_0 + t_1$. So from Fig 4.3 equivalent circuit, we have: ($V_0\ is\ DC\ source\ voltage$)

$$V_L = V_0 - V_C, v_d = V_0, v_i = V_C - v_L = 2V_C - V_0 \quad (35)$$

The relationship with switching period and voltage of capacitor and dc source is:

$$\frac{V_C}{V_0} = \frac{t_1}{t_1 - t_0} \quad (36)$$

The peak dc-link voltage across the inverter bridge is expressed in (34) and can be rewritten as

$$\hat{v}_i = V_C - V_L = 2V_C - V_0 = \frac{t}{t_1 - t_0} V_0 = B \cdot V_0 \quad (37)$$

$$\rightarrow B = \frac{t}{t_1 - t_0} \geq 1 \quad (38)$$

The output peak phase voltage from the inverter can be expressed as

$$\hat{v}_{AC} = M \cdot \frac{\hat{v}_i}{2} \quad (39)$$

B is the boost factor, where M is the modulation index. Using (38) and (39) can get the equation

$$\hat{v}_{AC} = MB \cdot \frac{V_0}{2} \quad (40)$$

From this equation, we know the output AC voltage can be controlled by the value of M and B, the boost factor [7].

5 Simulation Model

5.1 Simulink model of hardware circuit

Fig. 5.1 shows a three-phase inverter hardware model, there are consist of DC power supply, switches circuit, LC filter circuit and load circuit, both of them build with Simscape software.

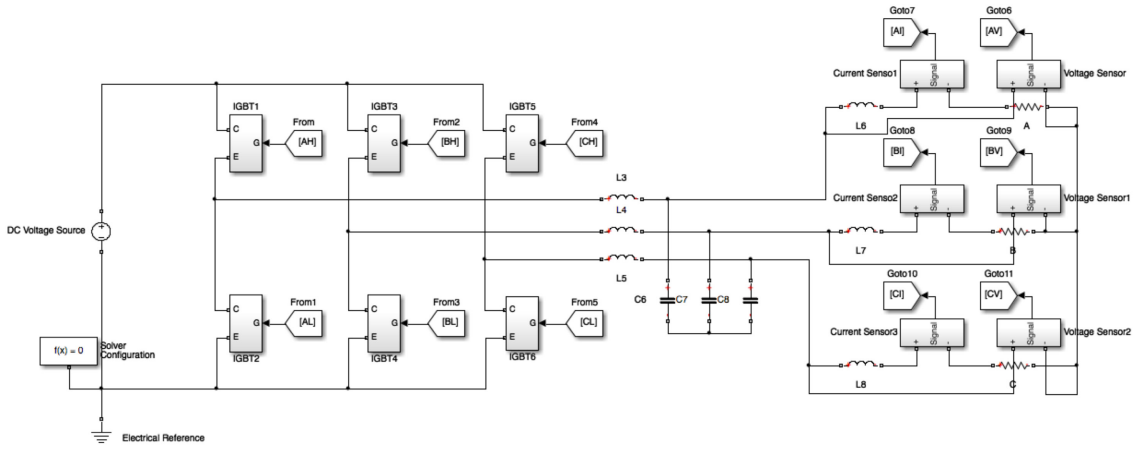

Fig. 5.1 Simulink model of three-phase full bridge inverter system

- *Switches circuit part*: The switches circuit is made of six ideal insulated-gate bipolar transistor (IGBT) model. In real world, the IGBT combines the simple gate-drive characteristics of metal–oxide–semiconductor field-effect transistor (MOSFET) with the high-current and low-saturation-voltage capability of bipolar transistor [9], so IGBT have both advantages of MOSFET and bipolar transistor, normally IGBT has been used in the high voltage and high current applications. Fig. 5.2 shows an ideal IGBT model and this model is built by Simscape.

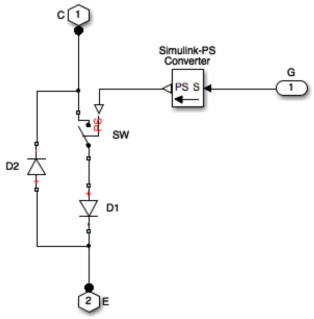

Fig. 5.2 The ideal IGBT model

- *Three-phase LC filter part*: In order to decrease the harmonic current, a three-phase LC filter is needed. There are three main harmonic currents produce by inverter: low frequency harmonics, switching frequency harmonics and high frequency harmonics. The LC filter is a second order filter which have -40dB/decade attenuation and its configuration circuit is shown in Fig. 5.3.

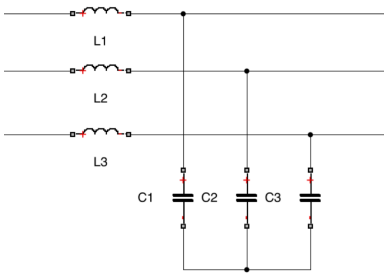

Fig. 5.3 Simulink model of LC filter

In this system, the fundamental frequency generate by inverter is *60 Hz*, therefore, the LC filter resonant frequency is calculated by equation (41):

$$f_0 = \frac{1}{2\pi\sqrt{LC}} = 60\ Hz \tag{41}$$

Let $L = 12mH$, the capacitor value C can be calculated by equation (41): $C = 586 \times 10^{-6}F = 586\mu F$. In the following simulations, all the LC filter value will be set as $L = 12mH\ and\ 586\mu F$.

5.2 Simulink model of SVPWM signal generator

The whole SVPWM control system is shown in Fig. 5.4 and it has six main subsystems: I. three-phase sinusoidal signal generator, II. Clarke's transformation, III. reference angel sector, IV. $T_1\ and\ T_2$ duration time calculation block, V. space vector modulation signal generator and VI. PWM signal generator. The SVPWM control system model is used to generate the SVPWM control signal for inverter and verify the output results are shown in chapter 6.

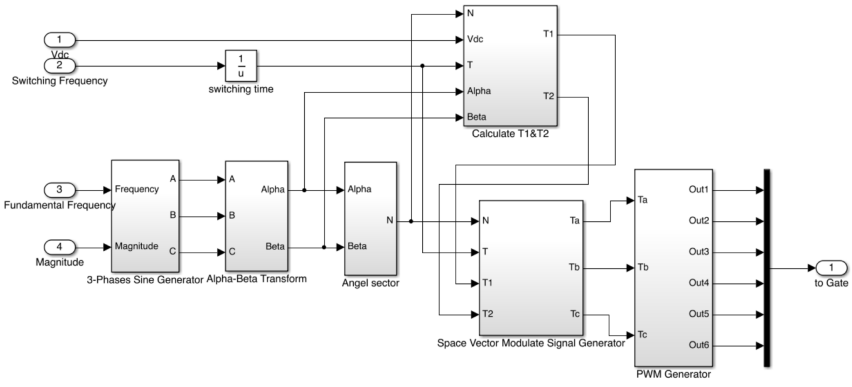

Fig. 5.4 SVPWM signal generator

Subsystem I: Fig. 5.5 (a) is shown the three-phase reference sinusoidal signal generator block. This block have variable input of frequency and magnitude, each of them can be adjusted independently. Therefore, the output three-phase voltage have same frequency and magnitude with 120° phase shift.

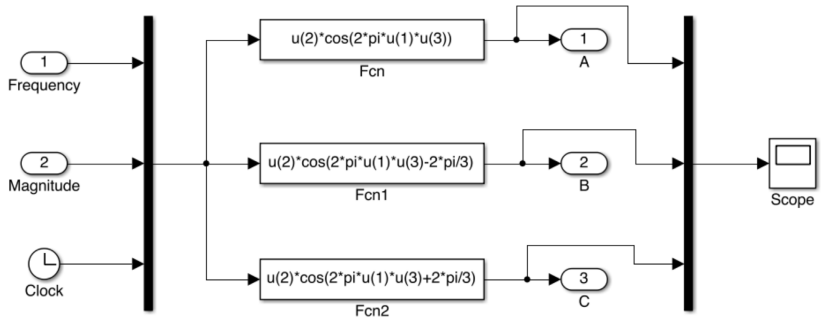

(a)

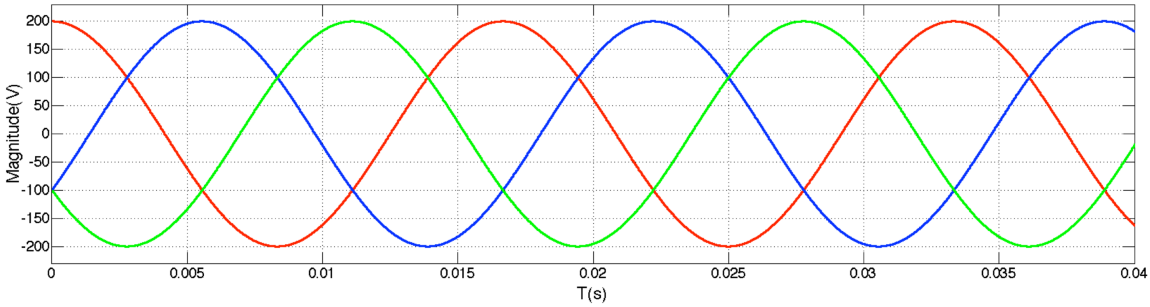

(b)

Fig. 5.5 Three-phase sinusoidal signal generator and output waveform

Subsystem II: Fig. 5.6 (a) shows the Clarke transformation block which is built depending on the equations (9) and (10). This transformation is used to converter three-phase *abc* voltage to two-phase $\alpha\beta$ voltage, then $\alpha\beta$ voltage will be used in *subsystem III* and *subsystem IV* to determine which sector is working and the value of time duration for six switches open or close.

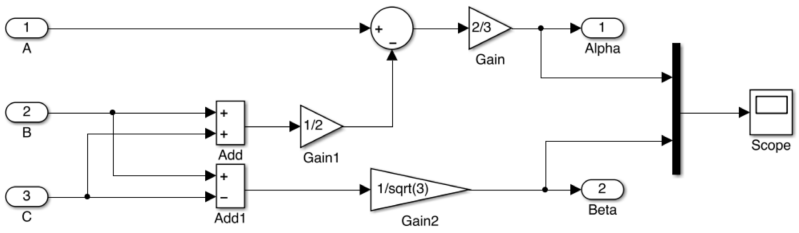

(a)

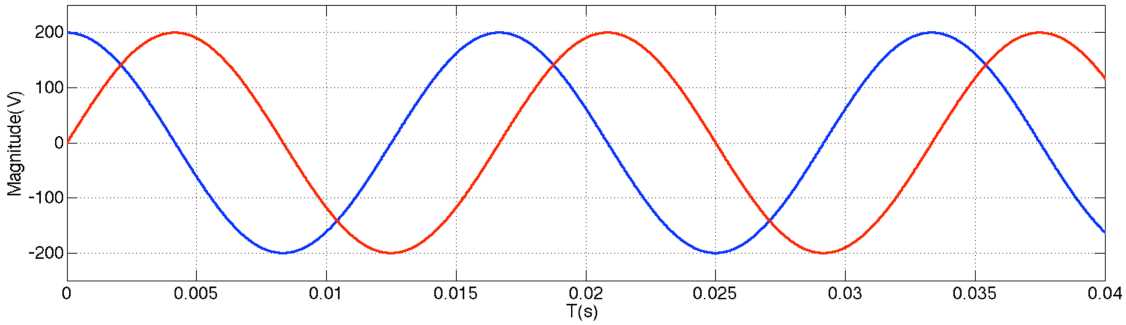

(b)

Fig. 5.6 Clarke transformation block and output waveform

Subsystem III: Fig. 5.7 (a) shows the calculation block, the value of N can be calculated by equations (27) and (28), and the relationship between N and sector is shown in Table 3 which can be used to determine which sector is working. Fig. 3.11 (b) is the sequence of the value of N that correspond with sector I to sector VI.

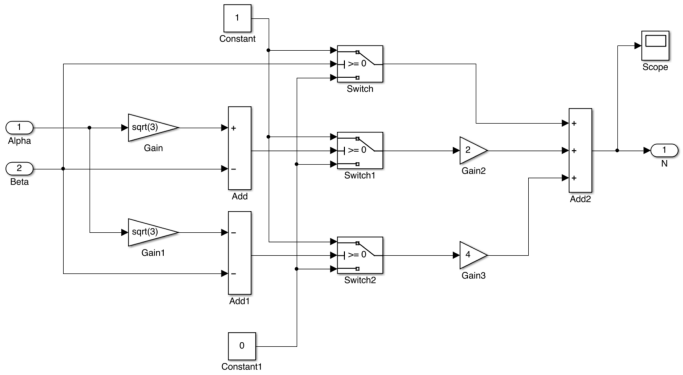

(a)

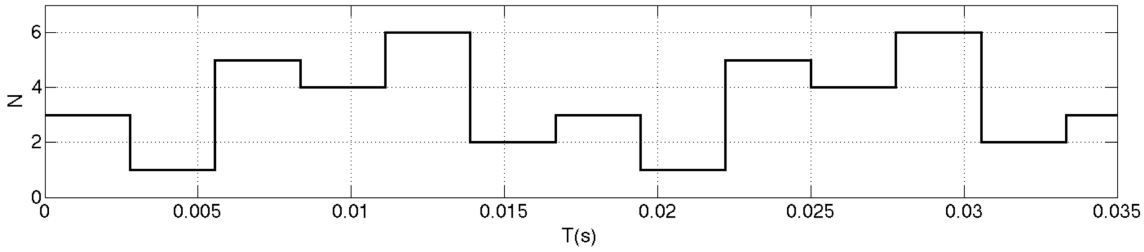

(b)

Fig. 5.7 Reference angel sector block

Subsystem IV: In Fig. 5.8, the switching time T_1 *and* T_2 has been calculated then selected bases on the value of N (T_1 *and* T_2 is variable in different vectors). The relationship

between N and T_1, T_2 is analyzed and calculated in equations (29), (30) and (31) and Table 4.

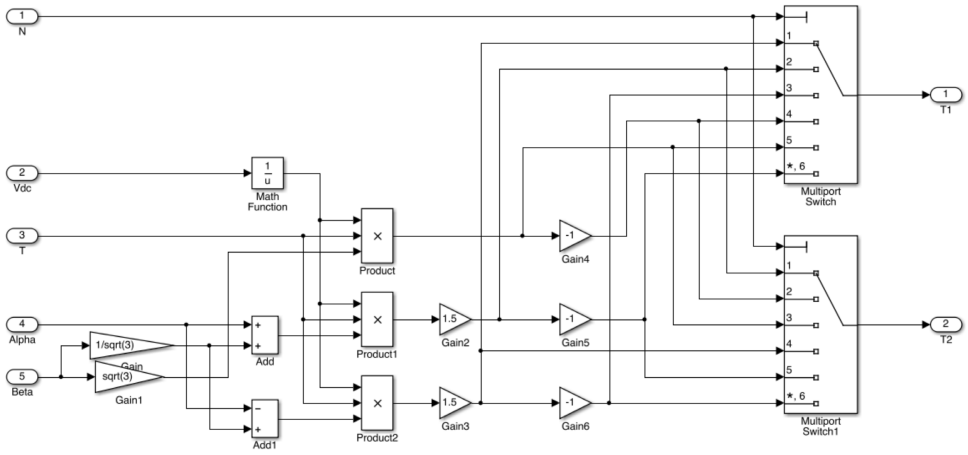

Fig. 5.8 T_1 *and* T_2 duration time calculation block

Subsystem V: Fig. 5.9 (a) is a calculation block which build by equation (32) and Table 5. The switching duration time T_a, T_b *and* T_c are calculated by equation (32) with the input value of T_1, T_2 *and* T_0 from *subsystem IV*, the output switching patterns sequences are depending on which sector working and selector will choose it as space vector modulation wave output. The space vector modulation waveform has a shape of saddle and shows in Fig. 5.9 (b), then will be compared to the PWM signal in next block.

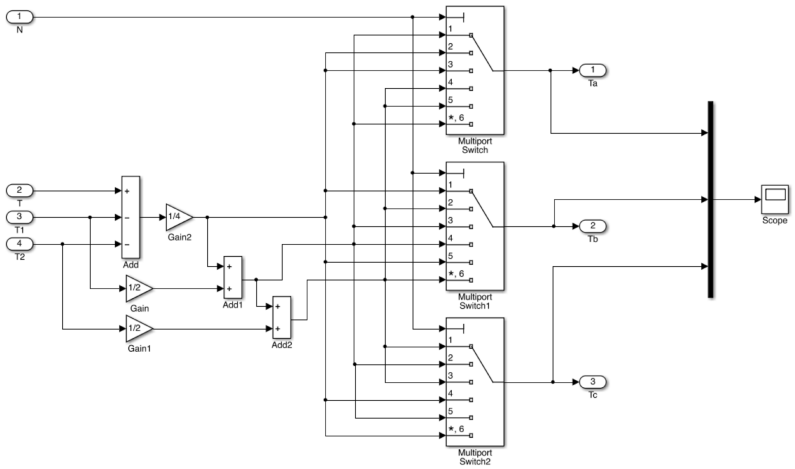

(a)

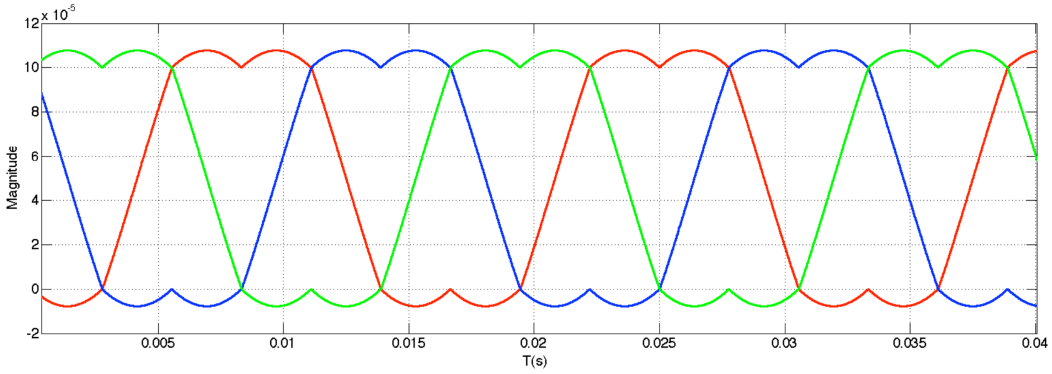

(b)

Fig. 5.9 Space vector modulation signal generator and the output waveform

Subsystem V: Fig. 5.10 (a) shows a PWM generate block, and input space vector modulation waveform will be compared to the PWM signal, then output the space vector PWM signal to six switches. Fig. 5.10 (b) is the comparison between PWM signal and space vector signal.

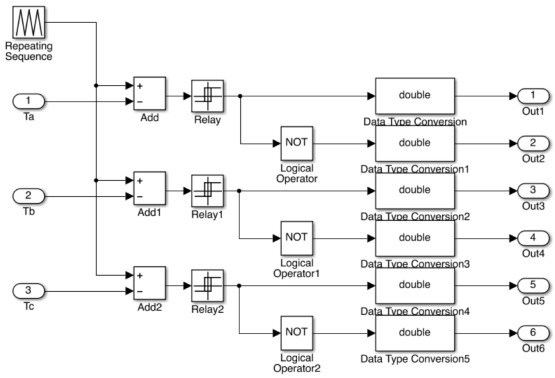

(a)

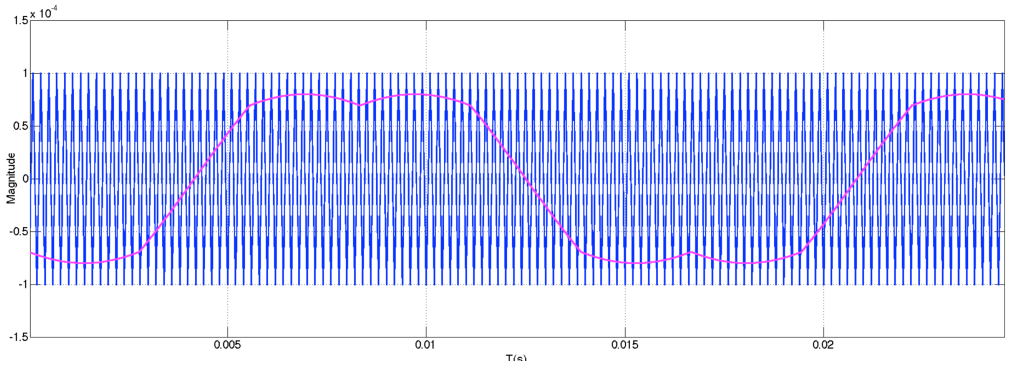

(b)

Fig. 5.10 PWM signal generator and the comparison waveform

5.3 Model building of Z-source inverter with modified SVPWM

Fig. 5.11 shows the structure of Z-source inverter, which is made of two capacitors and two inductances, the inductance L_1 and L_2 connected in series and capacitors C_1 and C_2 connected in X shape. Both of them create a two-port impedance network between dc source and three-phase inverter.

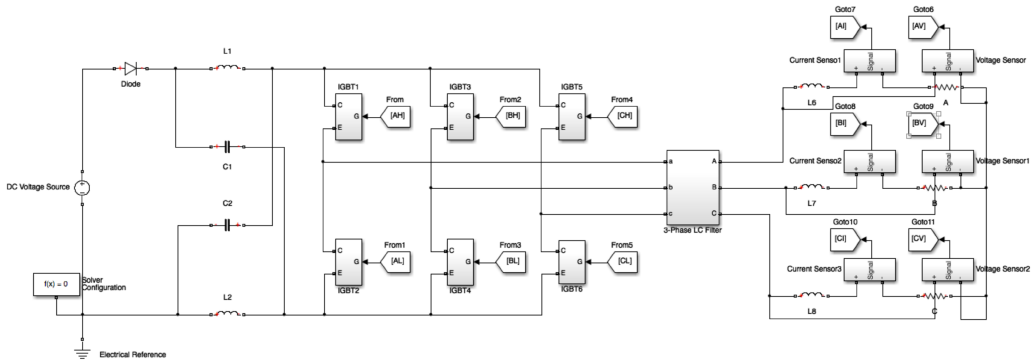

Fig. 5.11 Three-phase inverter with Z-source network

To generate the shoot-through time into the Z-source inverter control system, a pulse insert method is proposed in this report. Compare with other way to create the shoot-through time, this method is easier to control, and the results shown in chapter 6.

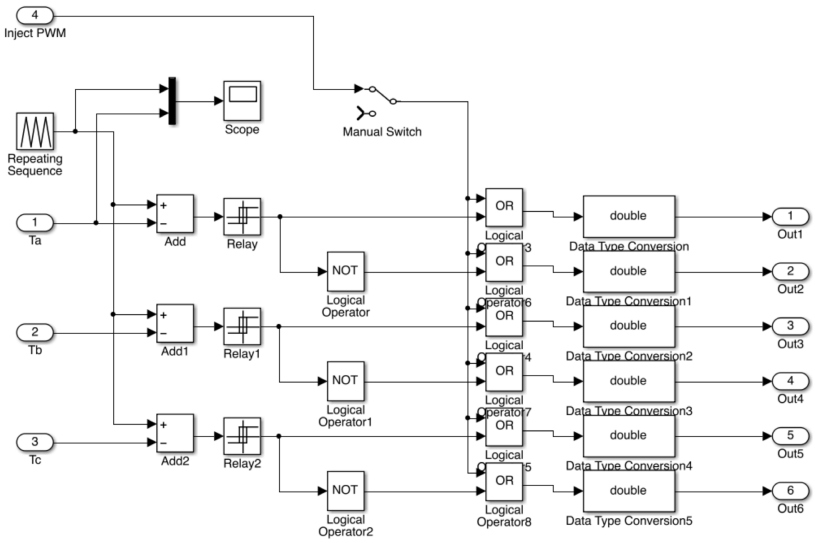

Fig. 5.12 Additional pulse signal inject into the SPWM/SVPWM signal and work together

6 Simulation Results

In this chapter, two models (SPWM and SVPWM) have been built with Matlab/Simulink and Simscape. In addition, the modified SPWM and modified SVPWM control method will be used in the Z-source network inverter. Both of their results have been compared and analyzed. In these models, all the electronic components are built by Simscape software, other control logic systems are built by Simulink software.

6.1 The SPWM simulation results

To verify the SPWM results, the simulations are conducted with initial system parameters which shows in Table 6.

Table 6 Initial system parameters setup

DC link voltage	Fundamental frequency	PWM frequency	Modulation index	Output LC filter	Load
$V_{DC} = 400V$	$f = 60Hz$	$f_{PWM} = 5000Hz$	$M.I_{\circ} = 0.8$	$L_f = 12mH,$ $C_f = 586\mu F$	$L_{load} = 5mH,$ $R_{load} = 10\Omega$

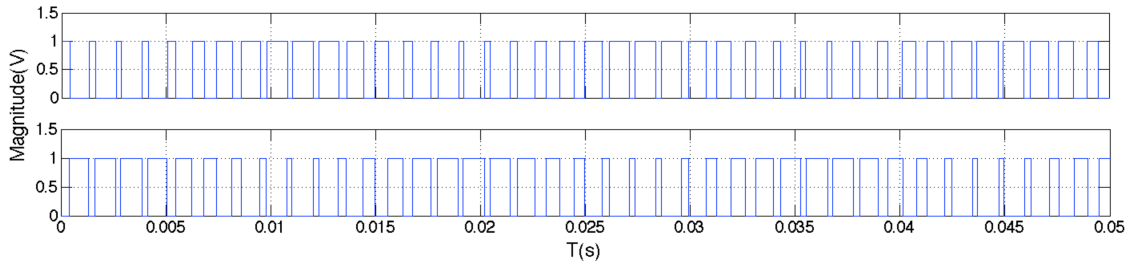

Fig. 6.1 SPWM control signal to one phase switches (upper and lower switches)

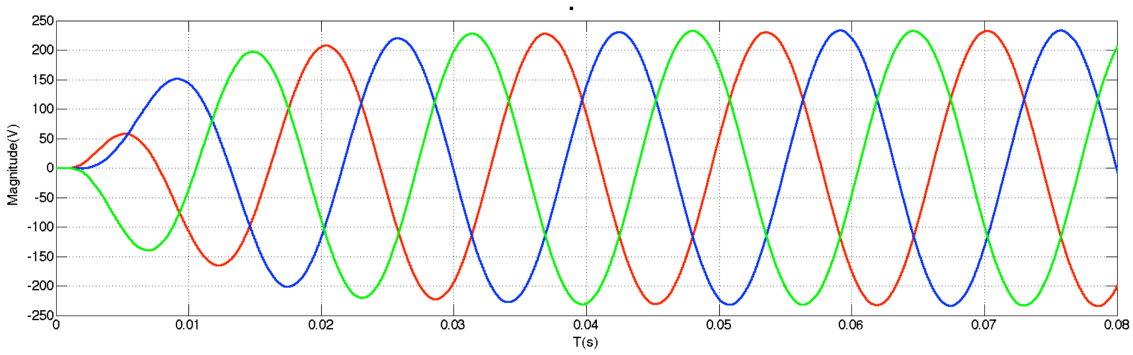

(a)

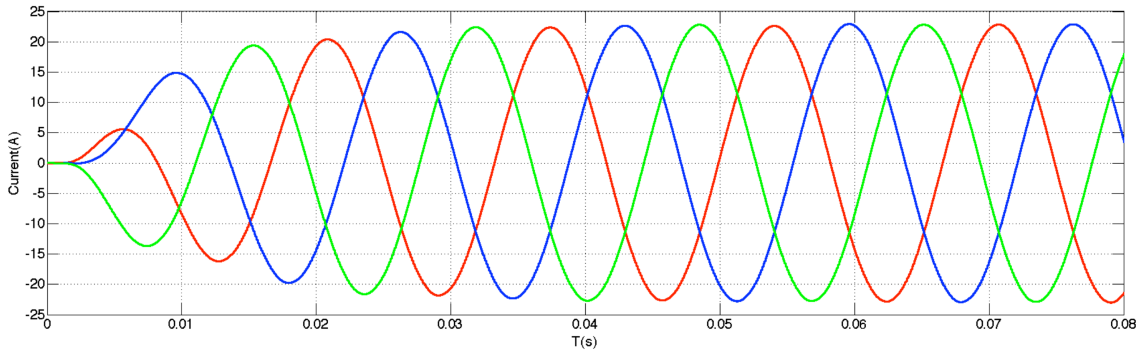

(b)

Fig. 6.2 Output voltage (a) and current (b) of SPWM after LC filter

Fig. 6.1 shows the SPWM control signal waveform for one phase switches, we can see pulses of the upper switch is contrary to the pulses of lower switch, because of the simulation is under ideal condition, no switches on/off delay, so the upper switch turn off and lower switch turn on at the same moment. Fig. 6.2 shows a good results for the output voltage and current, both of them are controlled to a good shape of sinusoidal waveform.

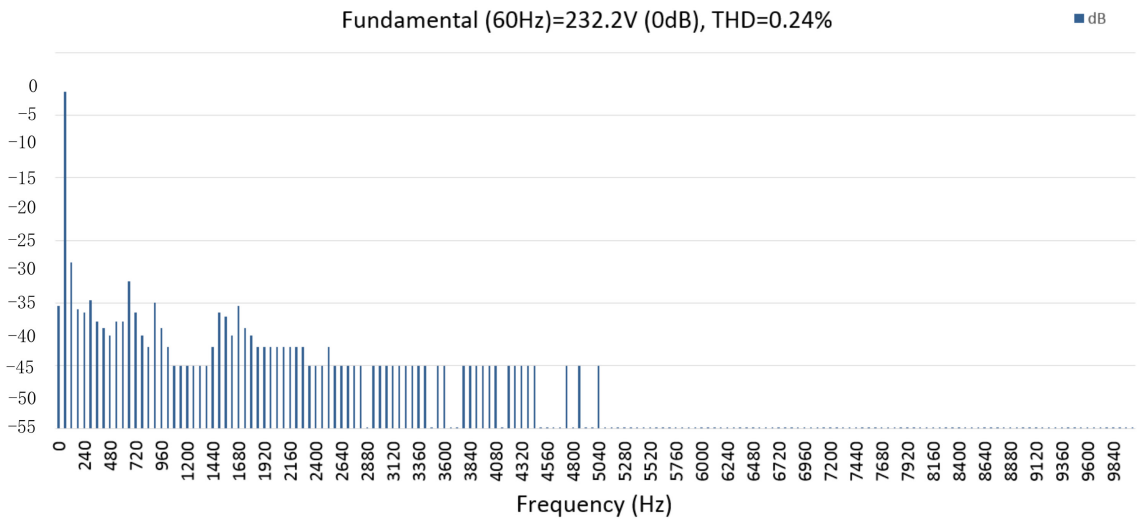

Fig. 6.3 FFT analysis of SPWM when MI = 0.8

From Fig. 6.3 shown above, we know the peak value of output phase voltage is 232.3V, THD = 0.24%. The main harmonics signal are 2^{nd} and 11^{th} harmonic (> -35dB).

Table 7 Output Voltages and THDs under different modulation index

M.I.	0.2	0.3	0.5	0.7	0.8	1.0	1.2
Output Vpp (V)	54.14	80.04	133.9	198.9	232.3	306.4	372.3
THD (%)	0.50	0.59	0.48	0.17	0.24	0.19	0.20

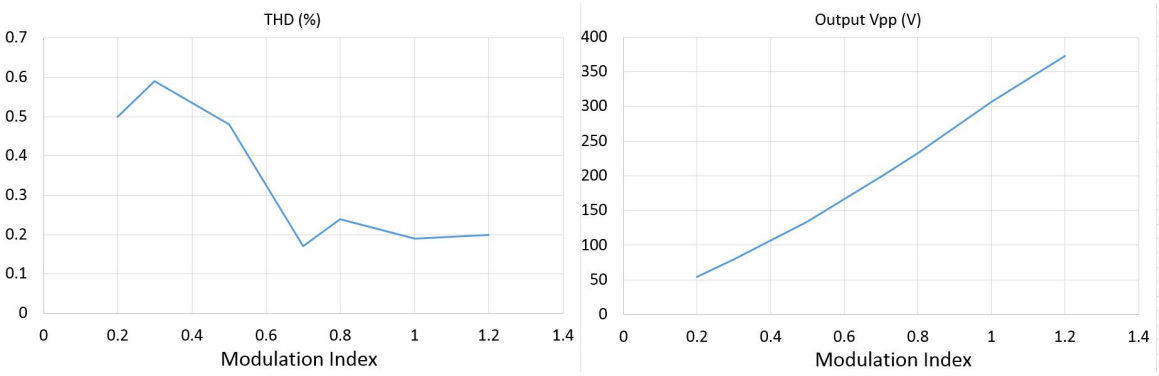

(a) (b)

Fig. 6.4 (a) Modulation index vs THD; (b) Modulation index vs output voltage

Fig. 6.4 shows the relationship between modulation index with THD and output voltage, from these curves we know the output voltage will increasing when the modulation index increase, and the THD has the smallest value when modulation index between 0.8 to 1.0. Therefore, to achieve better performance of inverter, the modulation index should be controlled between 0.5 and 1.0, and the output voltage have a linear relationship with modulation index.

6.2 The SVPWM simulation results

To verify the SVPWM results, the simulations are conducted with initial system parameters which shows in Table 8.

Table 8 Initial system parameters setup

DC link voltage	Fundamental frequency	PWM frequency	Modulation index	Output LC filter	Load
$V_{DC} = 400V$	$f = 60Hz$	$f_{PWM} = 5000Hz$	$M.I = 0.8$	$L_f = 12mH,$ $C_f = 586\mu F$	$L_{load} = 5mH,$ $R_{load} = 10\Omega$

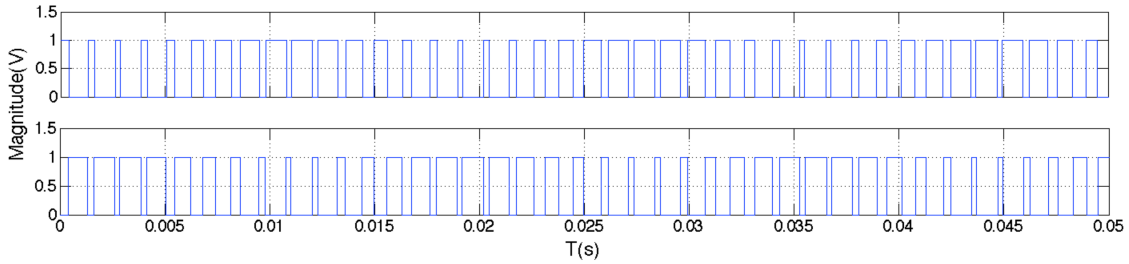

Fig. 6.5 SVPWM control signal to one phase switches (upper and lower switches)

Fig. 6.5 shows the SVPWM control signal waveform for one phase switches, we can see the control sequence is very similar with the SPWM control sequence. Fig. 6.6 shows a good results for the output voltage and current, both of them are controlled to a good shape of sinusoidal waveform.

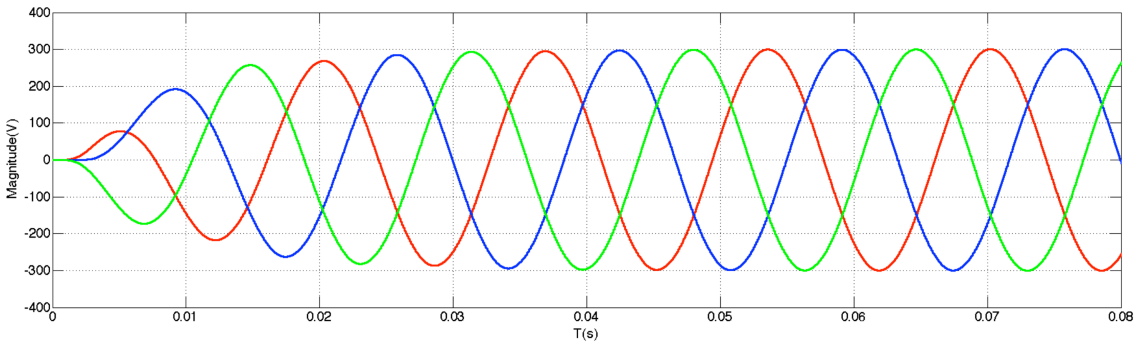

(a)

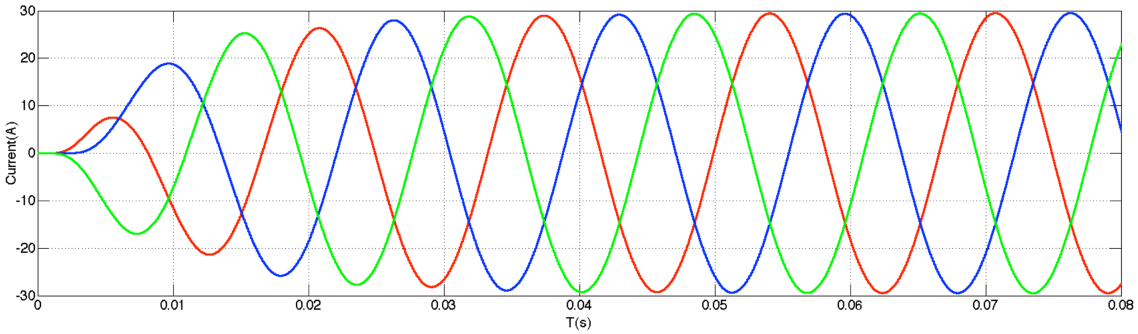

(b)

Fig. 6.6 Output voltage and current of SVPWM after LC filter

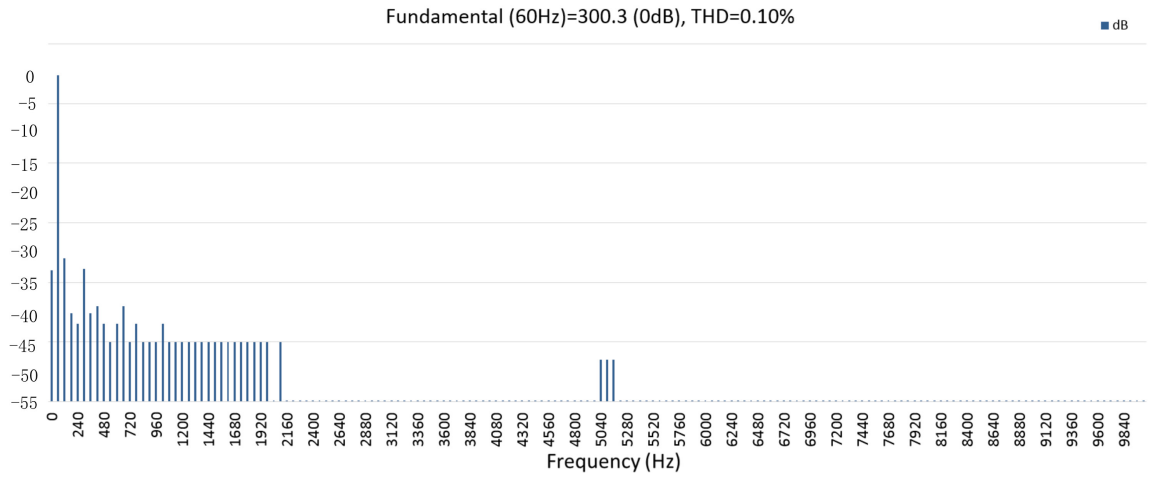

Fig. 6.7 FFT analysis of SVPWM when MI = 0.8

From the figures shown above, we know the peak value of output phase voltage is 300.3V, THD = 0.10% and less harmonics and higher dc link voltage utilization compare with the SPWM (output voltage $= 232.3\text{V}, \text{THD} = 0.24\%$) at same experimental condition. Also, the harmonics are almost concentrated in 2^{nd} and 5^{th} harmonic (> -35dB), other harmonics is less than SPWM control.

Table 9 Output Voltages and THDs under different modulation index

MI	0.2	0.3	0.5	0.7	0.8	1.0	1.2
Output Vpp (V)	28.24	89.49	164.6	226.6	300.3	361.2	406.8
THD (%)	0.49	0.34	0.70	0.12	0.10	0.14	0.13

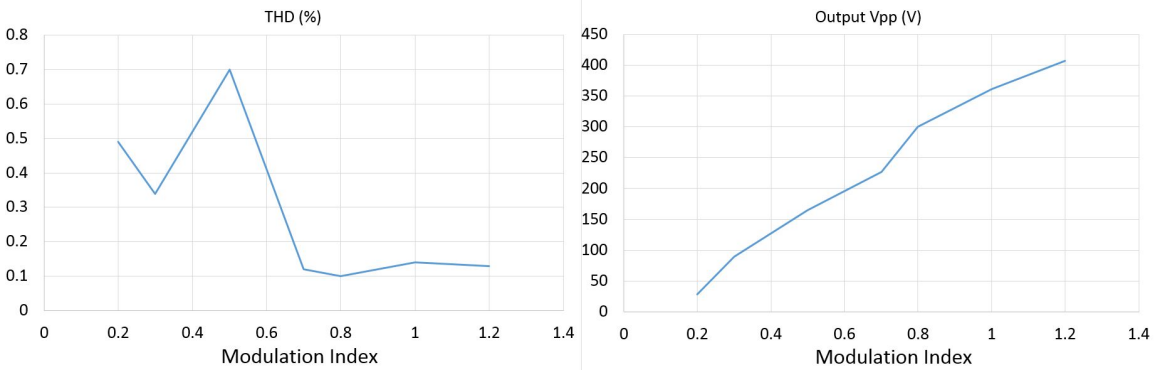

(a) (b)

Fig. 6.8 (a) Modulation index vs THD; (b) Modulation index vs output voltage

Fig. 6.8 shows the relationship between modulation index with THD and output voltage, from these curves we know the output voltage will increasing when the modulation index increase and the linear relationship is as the same with SPWM. The THD has the smallest value when modulation index between 0.6 to 1.0. Therefore, to achieve better performance of inverter, the modulation index should be controlled between 0.6 and 1.0. At the same dc input condition, SVPWM inverter can generate higher ac voltage (406.8V) when modulation index at 1.2 compare to SPWM. Moreover, SVPWM output waveform have less harmonics, therefore, to achieve better performance for inverter, we should choose SVPWM algorithm in the Z-source inverter.

6.3 The Z-source inverter with SVPWM control simulation results

In this model, we will running the simulation for the SVPWM control under Z-source network, at the same time, a PWM signal with $f = 4000\ Hz$ and duty cycle = 30% has been inserted to the control signal. The system parameters for this inverter are shown in Table 10:

Table 10 Initial system parameters setup

DC link voltage	Fundamental frequency	PWM frequency	Modulation index	Output LC filter	Load
$V_{DC} = 400V$	$f = 60Hz$	$f_{PWM} = 5000Hz$	$M.I = 0.8$	$L_f = 12mH,$ $C_f = 586\mu F$	$L_{load} = 5mH,$ $R_{load} = 10\Omega$

In this simulation, we will insert a PWM signal to the SVPWM sequence with Z-source network, the inserted PWM signal with $f = 4000\ Hz$ and duty cycle = 30%. In order to get the shoot-through time, the turned off switches will be turned on because of the inserted PWM signal has been added to the six switches.

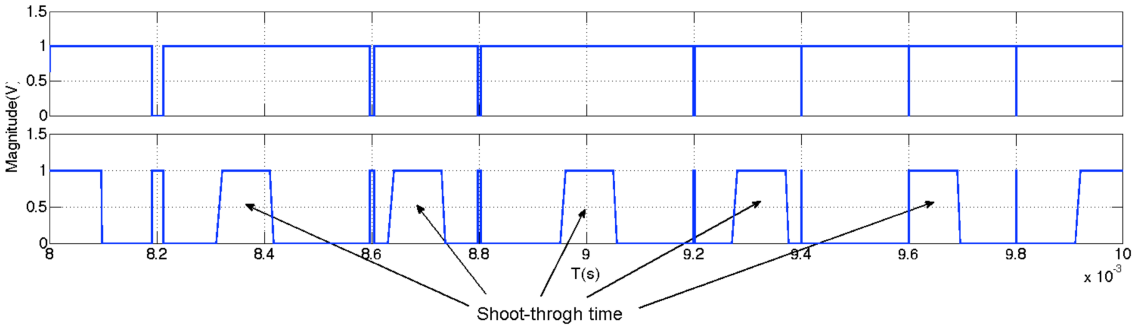

Fig. 6.9 Insert PWM sequence to the SVPWM signal and get the shoot-through time

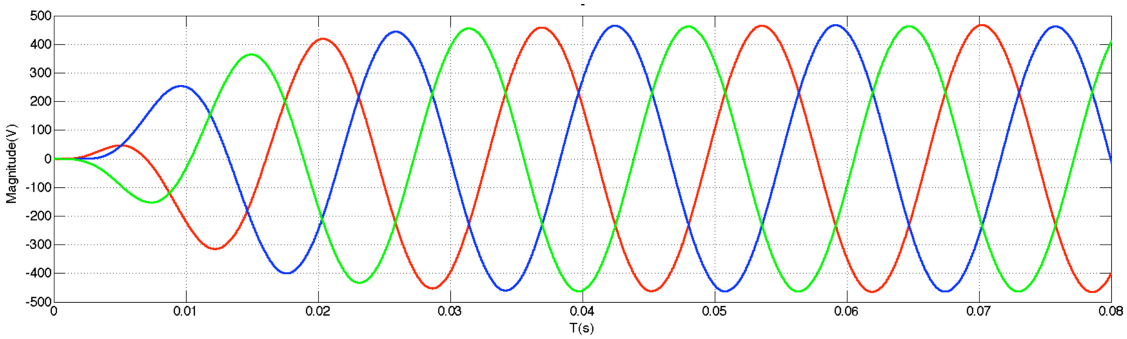

(a)

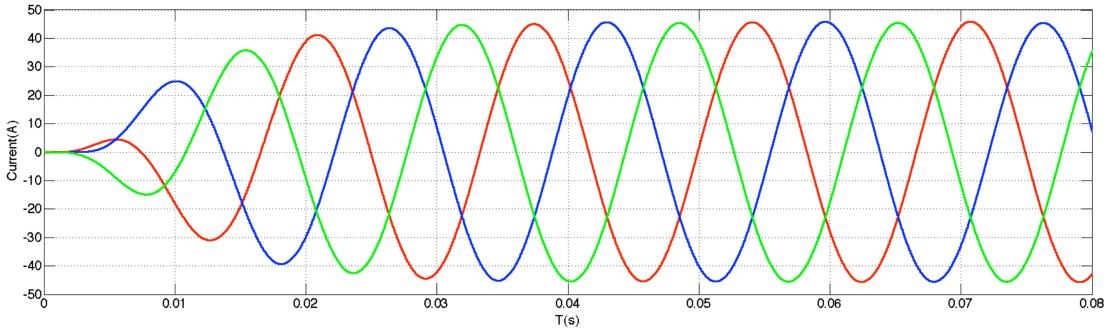

(b)

Fig. 6.10 Output voltage (a) and current (b) of Z-source inverter with modified SVPWM control

Fig. 6.10 shows a good results for the Z-source inverter with modified SVPWM control output voltage and current, both of them are controlled to a good shape of sinusoidal waveform.

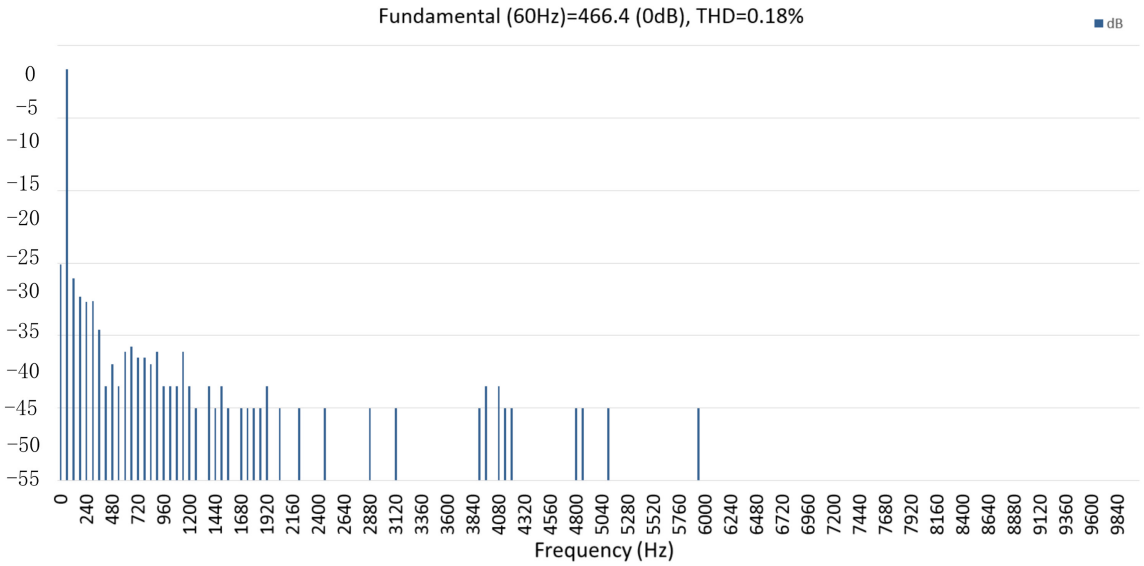

Fig. 6.11 FFT analysis of Z-source inverter with shoot-through time control

From the figures shown above, we know the peak value of output phase voltage is 466.4 and is higher than the output without using Z-source network, THD = 0.18% and it's little bit higher than the output without using Z-source network. However, in the real world, the less increasing value of THD can be ignored.

Table 11 Output Voltages and THDs with different frequency PWM inserted when MI=0.8, duty cycle = 30%.

Frequency	1000	1500	2000	2500	3000	3500	4000	4500	5000
Output Vpp (V)	443.4	442	451.5	468.2	448.9	447.7	466.4	447.1	451.7
THD (%)	0.30	0.18	0.25	0.32	0.13	0.08	0.18	0.69	1.87

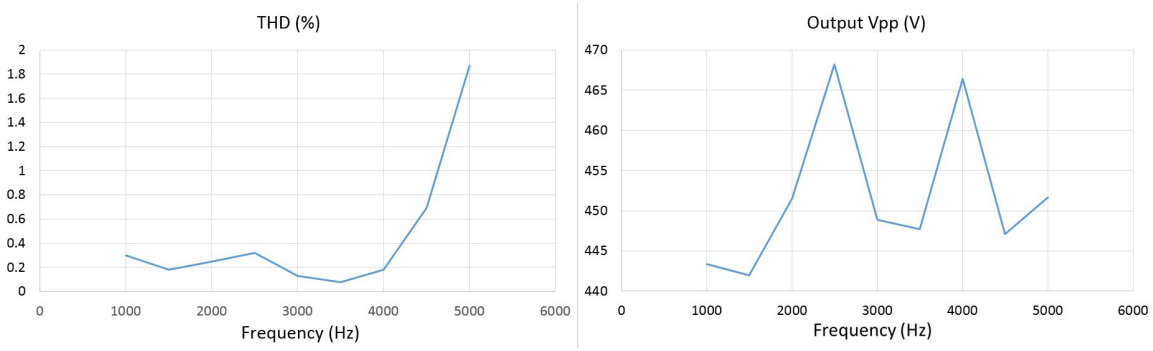

(a) (b)

Fig. 6.12 (a) Frequency vs THD; (b) Frequency vs output voltage

From Fig. 6.12, we know the effect of different frequency PWM inserted to the SVPWM control signal is no significant improvement for the output voltage, but the THD have significant affect from frequency. If frequency higher than carrier frequency ($f = 5000Hz$), the THD will increasing very fast.

Table 12 Output Voltages and THDs with PWM inserted when duty cycle = 30% under different modulation index

M.I	0.2	0.3	0.5	0.7	0.8	1.0	1.1	1.2	1.5
Output Vpp (V)	98.76	251.1	338	383.3	466.4	509	537.1	536.8	555.8
THD (%)	0.82	0.58	0.45	0.24	0.18	0.35	0.23	0.29	0.8

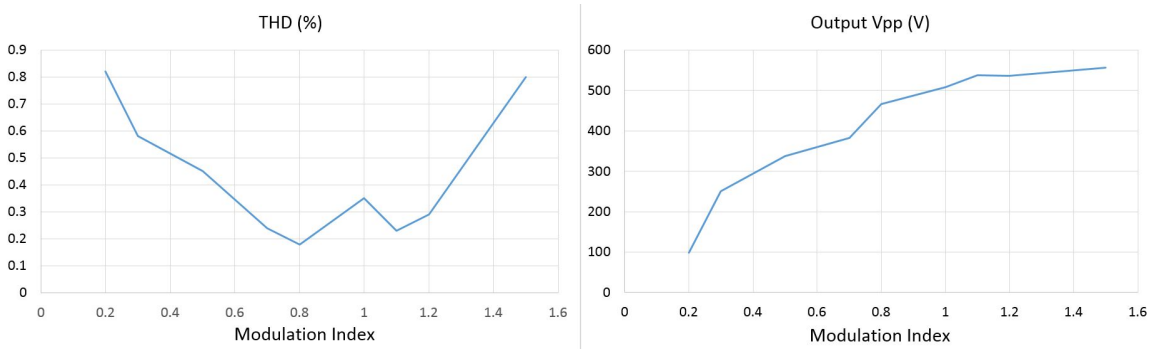

(a) (b)

Fig. 6.13 (a) Frequency vs THD; (b) Frequency vs output voltage

From Fig. 6.13, we can observe the THD have less value when the modulation index from 0.8 to 1.2, and the output voltage is increase when the modulation increase, even the modulation index = 1.5, the THD have a small value but the output can reach 556V, and it is over 1.5 times compare to SVPWM control without Z-source network when modulation index =1.

Table 13 Output Voltages and THDs under different duty cycle of PWM inserted when *f=4000, MI=1*

Duty cycle	1	10	15	20	25	30	35	40	45
Output Vpp (V)	378.5	404.8	419.7	440.6	492.4	509	519.4	502.3	218.3
THD (%)	0.15	0.16	0.16	0.38	0.22	0.35	0.30	0.68	0.24

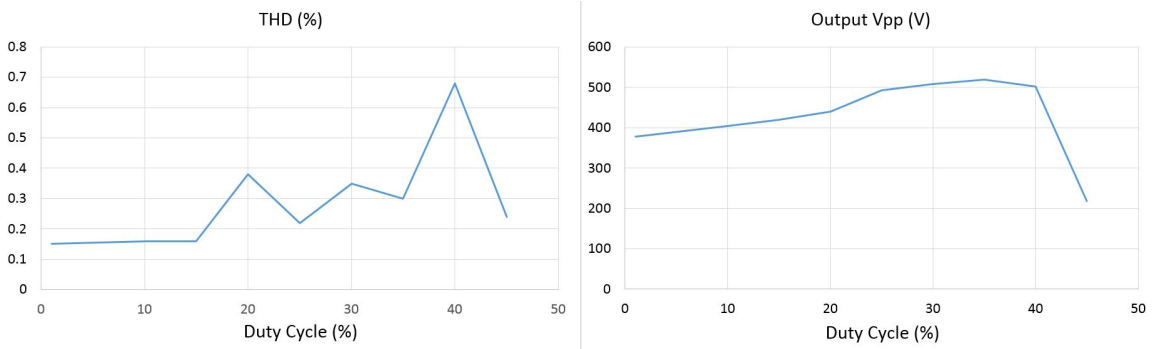

(a) (b)

Fig. 6.14 (a) Frequency vs THD; (b) Frequency vs output voltage

From Fig. 6. 14, we know the duty cycle of inserted PWM signal have a significant affect for the output voltage, Fig. 6.14 (b) shows when duty cycle over 40%, the boost feature will fail. Therefore, in order to use the boost feature in the Z-source inverter, the duty cycle of inserted PWM signal can't over 40%.

7 Conclusion

This report proposed a method for HEV/EV inverter application. In this report, the PWM sequences has been inserted to SVPWM control signal to achieve the shoot-through time in the Z-source network. To observe the effect when the PWM signal inserted, we used different frequency and duty cycle of PWM added to SVPWM control signal with different modulation index, and the experimental shows a significant results for boost dc-link voltage, and the output waveform have a good shape and less THD. Meanwhile, the output voltage can be easily boost the dc link voltage over 1.5 times to without Z-source network and have an acceptable output voltage and current waveform, so this Z-source inverter can overcome the main problem we encounter before, and can be used in the HEV/EV application and solar power applications.

However, the Z-source inverter still have two natural disadvantages:

- The Z-source inverter can't achieve bidirectional power flow without an additional switch. It's mean that if HEV/EV work under break/regeneration mode, the power generate from electric motor can't directly charge to the battery without the additional switch. If we want to work in the regeneration mode, an additional switch need to control so that the system cost will be increased.

- The Z-source voltage-fed inverter still have large total capacitance in the inverter system, because of the Z-source inverter need two large high rated voltage film capacitors with a large size to consist of the Z-source network.

Recently, some quasi Z-source inverters are developed very fast, especially the current-fed quasi Z-source inverter. This inverter can achieve bidirectional power flow with a diode, moreover, the current-fed quasi Z-source inverter have a small total capacitance in the system. Therefore, this novel quasi Z-source not only have the advantages that traditional Z-source inverter have, but also have these advantages: bidirectional power flow, low total system cost, reduce total capacitance and smaller system size.

8 References

[1] T.C. Martin, "*The Inventions, Researches and Writings of Nikola Tesla*", New Work: Electrical Engineer, 1894, pp. 9-11.

[2] "AC Induction Motors (ACIM) – Overview", Texas Instruments Incorporated, 2013. Available: http://www.ti.com/lsds/ti/apps/motor/ac_induction/overview.page

[3] "Permanent Magnet Synchronous Motors (PMSM) – Overview", Texas Instruments Incorporated, 2013. Available: http://www.ti.com/lsds/ti/apps/motor/permanent_magnet/overview.page

[4] M. Yano, S. Abe and E. Ohno. "History of Power Electronics for Motor Drives in Japan". p. 6, Fig 13. Retrieved 18 April 2012.

[5] B. Akin and N. Garg, "Scalar (V/f) Control of 3-Phase Induction Motors", Texas Instruments Incorporated, July 2013.

[6] C. Schauder, "Adaptive Speed Identification for Vector Control of Induction Motors without Rotational Transducers", IEEE Transactions on Industry Applications, vol. 28, No. 5, Sep/Oct 1992.

[7] B. Akin and M. Bhardwaj, "Sensored Field Oriented Control of 3-Phase Induction Motors", Texas Instruments Incorporated, July 2013.

[8] F. Z. Peng, "Z-Source Inverter", IEEE Transactions on Industry Applications, vol. 39, No. 2, pp. 504-510, March/April 2003.

[9] B. J. Baliga, "Fast-switching insulated gate transistors", IEEE Electron Device Letters, Vol. EDL-4, pp. 452-454, 1983.

[10] M. Kazmierkowski, R. Krishnan and F. Blaabjerg, *Control in Power Electronics*, CA: Academic Press, 2002, ch.10.

[11] S. R. Bowes and L. Yen-Shin, "The relationship between space-vector modulation and regular-sampled PWM", Industrial Electronics, IEEE Transactions on, vol. 44, pp. 670-679, 1997.

[12] R. Kennel, "Power Electronics Exercise: Pulse Width Modulation Methods", Technische Universität München, 2013.

[13] Phuong Hue Tran, "MATLAB/SIMULINK IMPLEMENTATION AND ANALYSIS OF THREE PULSE-WIDTH-MODULATION (PWM) TECHNIQUES", Boise State University, May 2012.

[14] Z. Mihailovic, "Appendix A: Rotating (D-Q) Transformation and Space Vector Modulation Basic Principles", Virginia Polytechnic Institute and State University, 1998.

[15] K. Kumar, P. Michael, J. John and S. Kumar, "SIMULATION AND COMPARISON OF SPWM AND SVPWM CONTROL FOR THREE PHASE INVERTER", ARPN Journal of Engineering and Applied Sciences, VOL. 5, NO. 7, JULY 2010.

[16] J. W. Jung, "PROJECT #2 Space vector PWM inverter", Mechatronic Systems Laboratory, OHIO STATE UNIVERSITY, 2005.

[17] Park, R.H., "Two-Reaction Theory of Synchronous Machines", AIEE Trans. No.48, 1929, pp.716-730 and no. 52, 1933, pp.352-355.

[18] K. Ahmed, S. Finney and B. Williams, “Passive Filter Design for Three-Phase Inverter Interfacing in Distributed Generation”, Electrical Power Quality and Utilisation, Journal Vol. XIII, No. 2, 2007.

[19] W. F. Zhang and Y. H. Yu, “Comparison of Three SVPWM Strategies”, JOURNAL OF ELECTRONIC SCIENCE AND TECHNOLOGY OF CHINA, VOL. 5, NO. 3, SEPTEMBER 2007.

[20] M. Olszewski, “EVALUATION OF THE 2010 TOYOTA PRIUS HYBRID SYNERGY DRIVE SYSTEM”, Oak Ridge National Laboratory, ORNL/TM-2010/253, May 2010.

[21] D. Neacsu, “SPACE VECTOR MODULATION –An Introduction”, the 27th Annual Conference of the IEEE Industrial Electronics Society, 2001.

[22] Q. Lei, F.Z. Peng and M.S. Shen, “Switched-coupled-inductor inverter”, Energy Conversion Congress and Exposition (ECCE), IEEE, Sep 2013.